Contributions to Mineralogy and Petrology (2018) 173:26
https://doi.org/10.1007/s00410-018-1454-5

ORIGINAL PAPER

Zircon ages in granulite facies rocks: decoupling from geochemistry above 850 °C?

Barbara E. Kunz[1,2] · **Daniele Regis**[1,3] · **Martin Engi**[1]

Received: 21 July 2017 / Accepted: 1 March 2018 / Published online: 8 March 2018

Abstract

Granulite facies rocks frequently show a large spread in their zircon ages, the interpretation of which raises questions: Has the isotopic system been disturbed? By what process(es) and conditions did the alteration occur? Can the dates be regarded as real ages, reflecting several growth episodes? Furthermore, under some circumstances of (ultra-)high-temperature metamorphism, decoupling of zircon U–Pb dates from their trace element geochemistry has been reported. Understanding these processes is crucial to help interpret such dates in the context of the *P–T* history. Our study presents evidence for decoupling in zircon from the highest grade metapelites (> 850 °C) taken along a continuous high-temperature metamorphic field gradient in the Ivrea Zone (NW Italy). These rocks represent a well-characterised segment of Permian lower continental crust with a protracted high-temperature history. Cathodoluminescence images reveal that zircons in the mid-amphibolite facies preserve mainly detrital cores with narrow overgrowths. In the upper amphibolite and granulite facies, preserved detrital cores decrease and metamorphic zircon increases in quantity. Across all samples we document a sequence of four rim generations based on textures. U–Pb dates, Th/U ratios and Ti-in-zircon concentrations show an essentially continuous evolution with increasing metamorphic grade, except in the samples from the granulite facies, which display significant scatter in age and chemistry. We associate the observed decoupling of zircon systematics in high-grade non-metamict zircon with disturbance processes related to differences in behaviour of non-formula elements (i.e. Pb, Th, U, Ti) at high-temperature conditions, notably differences in compatibility within the crystal structure.

Keywords Zircon · High-temperature metamorphism · Decoupling zircon characteristics · U–Pb dating · Th/U ratios · Ti-in-zircon thermometry

Introduction

Zircon is an accessory phase found in a large variety of rock types. While it is stable over a wide range of metamorphic conditions, modelling predicts growth mostly in restricted parts of a *P–T* path (e.g. Yakymchuk and Brown 2014; Kohn et al. 2015). For new metamorphic zircon to form in high-temperature (HT) metamorphic rocks, either the presence of a hydrous fluid or melt phase is required (e.g. Watson and Harrison 1983; Fraser et al. 1997; Tomaschek et al. 2003; Tichomirowa et al. 2005). In the absence of fluids, metamorphic zircon may form via solid-state (partial) recrystallisation (e.g. Schaltegger et al. 1999; Hoskin and Black 2000; Tomaschek et al. 2003; Rubatto et al. 2006) or by the breakdown of Zr-rich minerals (Fraser et al. 1997; Degeling et al. 2001; Bingen et al. 2004; Ewing et al. 2013; Pape et al. 2016).

Communicated by Timothy L. Grove.

Electronic supplementary material The online version of this article (https://doi.org/10.1007/s00410-018-1454-5) contains supplementary material, which is available to authorized users.

✉ Barbara E. Kunz
barbara.kunz@open.ac.uk

[1] Institute of Geological Sciences, University of Bern, Baltzerstrasse 1+3, 3012 Bern, Switzerland

[2] School of Environment, Earth and Ecosystem Sciences, The Open University, Walton Hall, Milton Keynes MK7 6AA, UK

[3] Geological Survey of Canada, Natural Resources Canada, 601 Booth St., Ottawa, ON, Canada

Numerous studies have made a contribution to unravel and understand the record of information preserved in metamorphic zircon (e.g. Roberts and Finger 1997; Vavra et al. 1999; Schaltegger et al. 1999; Hoskin and Black 2000; Rubatto et al. 2001, 2006; Williams 2001; Rubatto 2002; Hermann and Rubatto 2003; Möller et al. 2003; Tomaschek et al. 2003; McFarlane et al. 2005, 2006; Vonlanthen et al. 2012; Vorhies et al. 2013). Recent studies have improved our understanding of how to interpret metamorphic zircon in the context of the *P–T* evolution of rocks by modelling zircon growth during metamorphism (e.g. Kelsey et al. 2008; Kelsey and Powell 2011; Yakymchuk and Brown 2014; Kohn et al. 2015; for a recent review of zircon petrochronology, see Rubatto 2017). A number of studies have found that zircon chemical and isotopic signatures can be altered by various mechanisms: Pb can be locally lost (e.g. Mezger and Krogstad 1997; Geisler et al. 2002; McFarlane et al. 2005) or gained (e.g. McFarlane et al. 2005), or Pb can be redistributed at sub-micron scale (e.g. Kusiak et al. 2013a, b; Valley et al. 2014; Whitehouse et al. 2014; Peterman et al. 2016; Regis et al. 2017). Similarly, evidence of U-loss or -gain has been found (e.g. Geisler et al. 2002; Seydoux-Guillaume et al. 2015), as well as trace elements (e.g. REE) loss by leaching (e.g. Vonlanthen et al. 2012) or redistribution (e.g. Reddy et al. 2006; Timms and Reddy 2009; Piazolo et al. 2016). Mechanisms proposed as being responsible for these effects include metamictisation due to radiation damage (e.g. Nasdala et al. 2001; Ewing et al. 2003), annealing of radiation damage (e.g. Nasdala et al. 2002), fluid alteration (e.g. Geisler et al. 2002; Vonlanthen et al. 2012; Seydoux-Guillaume et al. 2015), crystal plastic deformation (e.g. Reddy et al. 2006; Timms and Reddy 2009; Timms et al. 2011), and annealing due to crystal lattice strain (e.g. Schaltegger et al. 1999).

Several studies on zircon from (ultra-)high-temperature (UHT) terrains show that decoupling of zircon ages from textures and/or geochemistry can occur (e.g. McFarlane et al. 2005; Flowers et al. 2010; Kusiak et al. 2013a, b; Whitehouse et al. 2014). The conditions and mechanisms that lead to the observed decoupling are far from being fully understood: metamictisation can contribute but does not appear to be a requirement (Whitehouse et al. 2014), and nm-sized Pb (and trace elements) clusters or patchy Pb distributions have been reported (Kusiak et al. 2013a, b; Whitehouse et al. 2014; Regis et al. 2017). So far, decoupling has been studied in zircon of Paleo-Proterozoic age only. Here we report decoupling in relatively young (~ 280 Ma) crystalline zircon from high-grade samples (> 850 °C) in the Ivrea Zone.

The Ivrea Zone (Fig. 1) is regarded as a section through the mid- to lower continental crust preserving a HT metamorphic imprint established during the late Palaeozoic (e.g. Berckhemer 1968; Mehnert 1975; Fountain 1976; Quick et al. 1995). Contrary to interpretations of early studies (e.g. Fountain 1989; Voshage et al. 1990; Sinigoi et al. 1991; Quick et al. 1994; Schnetger 1994; Henk et al. 1997), the now-accepted view is that the intrusion of mafic magmas into the lower crust was not the main cause for HT metamorphism (e.g. Barboza et al. 1999; Redler et al. 2012). There is no consensus, however, whether the regional HT metamorphism was first established during Variscan (collisional) metamorphism (e.g. Zingg et al. 1990; Schmid 1993) or caused by late Palaeozoic crustal thinning (e.g. Barboza and Bergantz 2000).

This study investigates the age and trace element variability in HT metamorphic zircon, with an emphasis on unravelling the origin of the large scatter of U–Pb dates and their decoupling from textures and trace element geochemistry in zircon from the highest grade (> 850 °C) granulite facies part of the Ivrea Zone. The continuous metamorphic field gradient from mid-amphibolite (650 °C) to granulite facies conditions (950 °C) exposed in the Ivrea Zone allows us to systematically study the evolution of zircon under increasing high-temperature conditions. Twelve samples collected along the metamorphic field gradient and four samples close to the contact of the mafic intrusion complex (Fig. 1) were investigated in detail. We analysed zircon core–rim proportions, internal textures, U–Pb ages, and trace element characteristics: Th/U ratios, REE, and Ti concentration.

Geological setting

The Ivrea Zone is a slice of Permian intermediate to lower continental crust of the Adriatic margin, today tilted by 90° and exposed in the Southern Alps of northern Italy (e.g. Zingg et al. 1990; Handy et al. 1999). The slice (ca. 120 by 14 km) exposes magmatic (Mafic Complex) and metamorphic rocks (Kinzigite Formation). To the northwest, the Ivrea Zone is bounded by the Insubric Line that separates it from units of the Western and Central Alps (Schmid et al. 1987). To the southeast, the Ivrea Zone is tectonically separated from an upper crustal block, the Serie dei Laghi/Strona–Ceneri Zone (Handy 1987, 1999; Boriani et al. 1990; Mulch et al. 2002a, b).

The Mafic Complex is an intrusive body consisting mainly of gabbro, norite and diorite with subordinate granite and tonalite (e.g. Quick et al. 2003; Rivalenti et al. 1975, 1981; Sinigoi et al. 1996). It was formed by magmatic underplating during the Permian extensional regime between ~ 290 and 280 Ma (e.g. Peressini et al. 2007; Sinigoi et al. 2011). The main intrusive phase has been dated on zircon by Peressini et al. (2007) at 288 ± 4 Ma, with locally earlier magmatic activity at ~ 295 Ma (Sinigoi et al. 2011) and 314 ± 5 Ma (Klötzli et al. 2014). In the northern part of the Ivrea Zone, the Finero mafic–ultramafic body is characterised by a range of Permian U–Pb zircon dates (290–250 Ma)

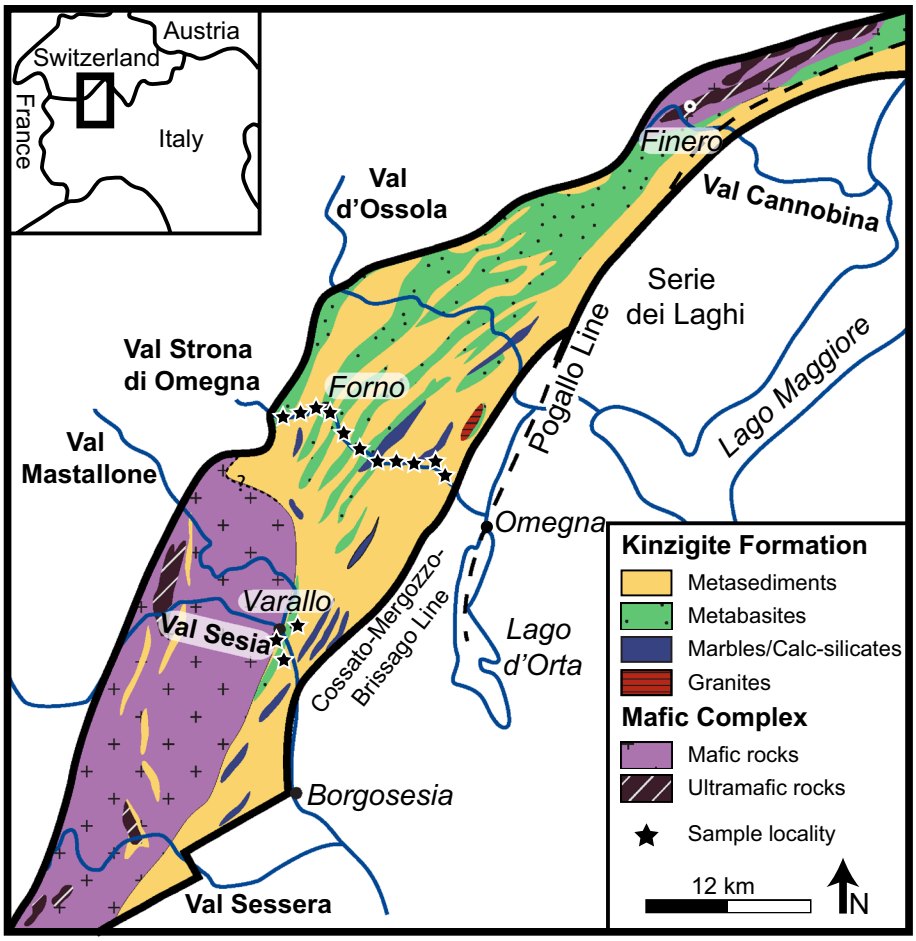

Fig. 1 Geological overview map of the Ivrea Zone, Southern Alps (N-Italy). Stars indicate sample localities in Val Strona di Omegna and Val Sesia. The map is based on Zingg (1980), Bigi and Carrozzo (1990), and Rutter et al. (2007)

as well as younger zircon intrusion ages of 232 ± 3 Ma and late fluid-related recrystallisation between ~220 and 200 Ma (Zanetti et al. 2013; Schaltegger et al. 2015; Langone et al. 2017).

The Kinzigite Formation mainly consists of metasedimentary rocks interlayered with metabasic rocks (e.g. Bertolani 1968). A continuous metamorphic field gradient from mid-amphibolite to granulite facies conditions is best exposed along Val Strona di Omegna, in the central Ivrea Zone (e.g. Zingg 1978; Schmid 1993; Henk et al. 1997; Redler et al. 2012; Kunz et al. 2014). The metamorphic field gradient is thought to reflect protracted heating during the late Palaeozoic, with a HT period in the Carboniferous/Permian (Schmid 1993; Henk et al. 1997). Owing to a pervasive thermal overprint during Permian regional high-grade metamorphism little information is preserved in the Ivrea Zone of its previous history. Polyphase deformation predating the Permian mafic intrusion (Rutter et al. 2007) and the presence of locally preserved kyanite relics (Bertolani 1959; Capedri 1971; Boriani and Sacchi 1973; Handy 1986) have been related to collision during the Variscan orogeny.

Based on phase equilibrium modelling in Val Strona di Omegna, *P*–*T* estimates for peak metamorphic conditions range from ~3.5–6.5 kbar at 650–730 °C in mid-amphibolite facies samples to 10–12 kbar at > 900 °C in the highest grade samples (Redler et al. 2012). Temperatures of 900–950 °C for peak conditions in the granulite facies have been derived from Zr-in-rutile thermometry (Luvizotto and Zack 2009; Ewing et al. 2013). Several studies have presented field and petrological evidence that the Mafic Complex was not the heat source for regional granulite facies metamorphism (Barboza et al. 1999; Barboza and Bergantz 2000; Redler et al. 2012). A local contact aureole of 1–3 km around the mafic intrusion is observed in Val Sesia (Fig. 1), overprinting earlier high-grade mineral assemblages (Barboza et al. 1999; Redler et al. 2012). Furthermore, the northeastern contact of the intrusion crosscuts earlier metamorphic isograds in the surrounding country rocks (e.g. Zingg et al. 1990; Barboza et al. 1999), suggesting a previous regional metamorphic event, possibly related to Variscan crustal thickening (Zingg et al. 1990; Schmid 1993). Geochronological studies show that the earliest phase of regional metamorphism is coeval with the first intrusive phase of the Mafic Complex at c. 315 Ma (Ewing et al. 2013; Klötzli et al. 2014). However, the range of HT metamorphic zircon dates (316–258 Ma; e.g. Vavra et al. 1999; Ewing et al. 2013) exceeds the range

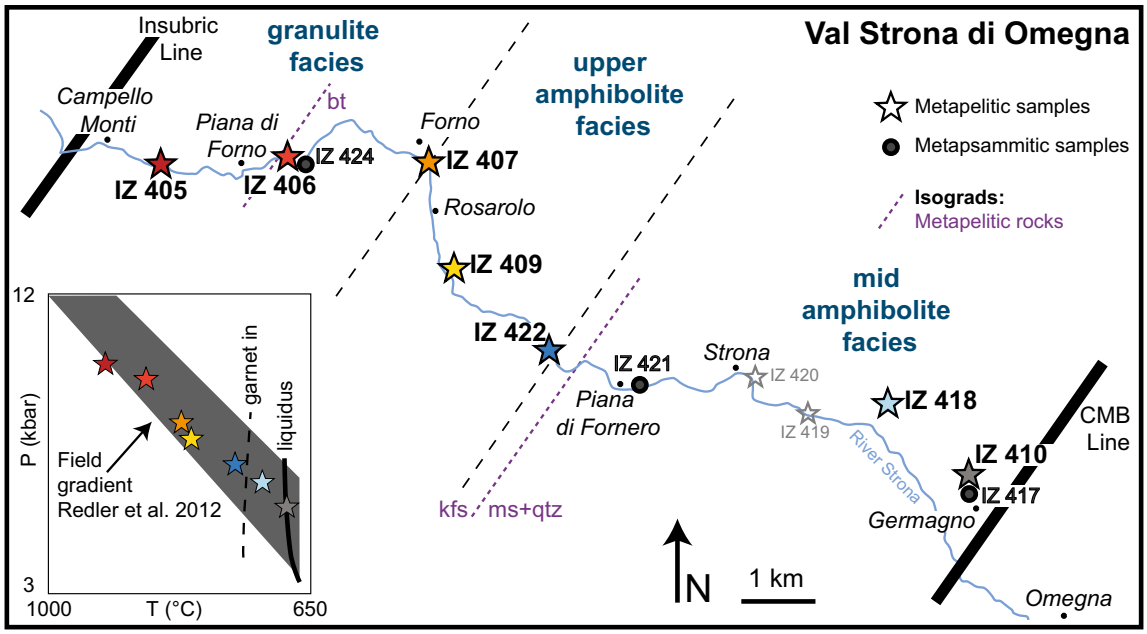

Fig. 2 Schematic map of Val Strona di Omegna, with metamorphic facies and mineral isograds. Stars show localities of metapelite samples, circles indicate metapsammite samples (see also Table 1). Grey stars indicate samples that yielded no zircon. Mineral isograds and metamorphic field gradient are taken from Redler et al. 2012. Facies boundaries are based on mineral isograds (cpx-in and opx-in) in metabasic rocks (Kunz et al. 2014)

of magmatic zircon (315–280 Ma, e.g. Peressini et al. 2007; Klötzli et al. 2014) by about 20 Myr. Previous studies by Vavra et al. (1999) and Ewing et al. (2013) interpreted the youngest zircon ages as possible resetting pre-existing Variscan (?) regional metamorphic ages. However, the driving mechanism behind this resetting process remains unclear, and we note that the young generation of ages is the most abundant fraction of the zircon age population.

Materials and methods

Sample material

Previous studies have shown how bulk rock composition can control the amount and possible timing of zircon crystallisation/dissolution (e.g. Rubatto et al. 2006; Kelsey et al. 2008; Kelsey and Powell 2011; Yakymchuk and Brown 2014; Kohn et al. 2015). Therefore, to understand the evolution of zircon growth along the continuous metamorphic field gradient in Val Strona di Omegna and avoid misinterpretations due to compositional differences, we collected nine aluminous metapelitic samples (Figs. 1, 2). The samples were collected from the same outcrops or in close vicinity of the sample locations of the metapelites modelled by Redler et al. (2012, 2013). This allowed us to infer approximate *P–T* conditions for our samples (Table 1). Two samples (IZ 419 and IZ 420) did not yield zircon during mineral separation and, therefore, are not further discussed. For comparison, three metapsammite samples (Fig. 2) from low- to high-grade were also sampled and analysed. In Val Sesia, where the intrusion of the Mafic Complex caused a narrow contact aureole, two samples were collected directly at the contact and two at some distances (~500 m) from the intrusive contact (Fig. 1).

Seven metapelite samples were collected in Val Strona di Omegna (Fig. 2, S1 Online Resource 1). Along the metamorphic field gradient the metapelites evolve from foliated micaschists to migmatites (Fig. S1 Online Resource 1). Sample IZ 407 originates from the Rosarolo shear zone and shows a mylonitic foliation. The mineral assemblages (Table 1; Fig. S1 Online Resource 1) in metapelites evolve from biotite, muscovite, fibrolitic sillimanite, plagioclase, and quartz (at mid-amphibolite facies) to garnet, prismatic sillimanite, biotite, K-feldspar, plagioclase, and quartz (in the upper amphibolite facies) and garnet, prismatic sillimanite, biotite, K-feldspar, plagioclase, quartz, and rutile at granulite facies. Minor minerals include ilmenite, apatite, zircon, monazite, rutile, hematite and xenotime.

The samples from Val Sesia have similar mineral assemblages as those at upper amphibolite facies in Val Strona di Omegna (Table 1), with the addition of cordierite in sample IZ 415. Mid-amphibolite facies metapsammites are composed of quartz, plagioclase, biotite, and sparse K-feldspar (sample IZ 417) with minor muscovite, sillimanite, and garnet (sample IZ 421). Granulite facies sample IZ 424 contains

Table 1 Summary of investigated samples sorted by locality and increasing metamorphic grade

Sample	Lithology	Coordinates		Locality	Mineral assemblage		Metamorphic facies	Peak *P–T* conditions from the literature		Zircon grains investigated by CL images
		E	*N*		Major	Minor		T (°C)	P (kbar)	
Val Strona di Omegna										
IZ 410	Metapelite	452144	5082832	Germango	Qtz + Pl + Bt + Ms + Sil	Ap + Zrn + Mnz	mA	< 640–730	< 3.5–8.4	183
IZ 417	*Metapsammite*	*452132*	*5082856*	*Germango*	*Qtz + Pl + Bt + Kfs*	*Zrn + Ap + Xtm + Hem + Mnz + Py*	*mA*	*720–785*	*5.8–10*	*209*
IZ 418	Metapelite	451425	5083567	Loreglia	Qtz + Pl + Bt + Ms + Sil	Zrn + Mnz + Ap + Hem + Py	mA	700	7.5	242
IZ 419	Metapelite	450049	5083675	Ponte di Romana	Bt + Sil + Qtz + Pl + Ms	Tur + Mnz + Gr + Xtm + Py + Hem + Ilm + Ap + Gr + (Zrn)	mA	–	–	2
IZ 420	Metapelite	449464	5084052	Strona	Pl + Qtz + Bt + Ms + Sil + Grt	Tur + Mnz + Gr + Ilm + Ap + Xtm + Py + (Zrn)	mA	–	–	5
IZ 421	*Metapsammite*	*447919*	*5083871*	*Piana di Fornero*	*Qtz + Pl + Bt + Ms + Sil + Grt*	*Zrn + Mnz + Ap + Gr + Ilm + Xtm + Hem*	*mA*	*650–730*	*3.5–8.4*	*122*
IZ 422	Metapelite	446714	5084462	Marmo	Pl + Qtz + Grt + Bt + Kfs + (Ms) + Sil	Zrn + Ap + Mnz + Hem + Gr + Py	uA	730–800	5.7–9.6	198
IZ 409	Metapelite	445455	5085396	Grampi	Qz + Pl + Grt + Bt + Kfs + Sil	Zrn + Mnz + Ap + Ilm + Py + Hem + Gr + **Rt?**	uA	810–850	6–10	163
IZ 407	Metapelite	445033	5086759	Otra	Qz + Grt + Bt + Sil + Pl + Kfs	Zrn + Ap + Gr + **Rt** + Py + Ilm + Mnz	uA	750–790	7–7.9	101
IZ 424	*Metapsammite*	*443097*	*5087055*	*Piana di Forno*	*Qtz + Pl + Grt + Kfs + (Bt)*	*Zrn + **Rt** + Gr + Hem + Ap + Mnz*	*G*	*830–910*	*9.6–11*	*176*
IZ 406a	Restite	442974	5087039	Piana di Forno	Qz + Gr + Pl + Sil + Bt + Kfs	**Rt** + Zrn + Mnz*	G	820–869	7.3–11.2	205
IZ 406b	Leucosome	442974	5087039	Piana di Forno	Qz + Pl + Kfs + Grt + Sil	**Rt** + Zrn + Mnz*	G	820–870	7.3–11.3	292
IZ 405	Metapelite	441652	5086809	Valdo	Grt + Qz + Pl + Sil + Kfs + Bt	Zrn + **Rt** + Gr + Mnz + Ilm + Py	G	> 870	< 9.5	276
Val Sesia										
IZ 416	Metapelite	442757	5074072	Varallo	Pl + Qtz + Bt + Kfs + Sil + Grt + (Ms)	Zrn + Ilm + Gr + Ap + Mnz + Xtm + Py	uA	–	–	63
IZ 415	Metapelite	442420	5072489	Crevola	Qtz + Pl + Kfs + Grt + Bt + Sil + Crd	Zrn + Mnz + Ilm + Hem + **Rt** + Ap + Gr	uA	820–862	4.7–6.9	51
IZ 411	*Metapsammite*	*442200*	*5073359*	*Crevola*	*Qtz + Pl + Grt + Kfs + Bt + (Sil)*	*Zrn + Mnz + Ap + Py + Gr + Hem + Ilm + **Rt?***	*uA*	*820–860*	*4.7–6.7*	*188*
IZ 412	Leucosome	442174	5073354	Crevola	Qtz + Pl + Kfs + Grt + Bt	**Rt** + Mnz + Ap + Ilm + (Rt) + Mnz + Hem + Py	uA	820–861	4.7–6.8	100

GPS coordinates are given in WGS84 reference system

Italic: metapsammite samples, bold: presence of rutile in the peak mineral assemblage

mA mid-amphibolite facies, *uA* upper amphibolite facies, *G* granulite facies. *P–T* estimates (phase equilibrium modelling) from the literature (Redler et al. 2012, 2013) are given from nearby localities

*Mnz in sample IZ 406 occurs only as inclusions in garnet

quartz, plagioclase, garnet, K-feldspar and minor biotite. Accessory phases in the metapsammites are the same as in the metapelites.

Zircon in all samples occurs abundantly in the matrix, in biotite, and sillimanite as well as occasionally in garnet. In samples IZ 405, IZ 406a and IZ 406b and IZ 407, rutile is present as fresh grains (up to 500 µm diameter) included in garnet, sillimanite, and in the matrix.

Methods

After sample disintegration using high-voltage pulse power fragmentation in a Selfrag lab system, zircon grains were separated by magnetic and heavy liquid mineral separation. Substantial amounts of good quality (idiomorphic, transparent) zircon were separated from the 250–64 µm grain size fraction of all but two samples (IZ 419 and IZ 420). Zircon grains were handpicked, mounted into acryl discs, and polished to expose their near-equatorial grain sections. To analyse internal textures and target potential locations for LA-ICP-MS spots, cathodoluminescence (CL) images were produced using a VPSE detector on the ZEISS EVO 50 scanning electron microscope at the Institute of Geological Science in Bern.

U–Pb ages, Ti and REE concentrations were measured by LA-ICP-MS at the University of Bern with a GeoLas-Pro 193 nm ArF Excimer laser system (Lambda Physik) and an Elan DRC-e quadrupole mass spectrometer (Perkin Elmer). Ablation was achieved using an energy density of 2.5 J/cm^2 with a repetition rate of 9 Hz using a spot size of 44 or 32 µm. Aerosol transport was attained with a mixture of He (1 l/min) and H_2 (0.08 l/min). Instrument tuning for U–Pb measurements was optimised for heavy masses; oxide production (ThO^+/Th^+) was always maintained below 0.5%. For trace element measurements the instrument was optimised to achieve equal sensitivity over all measured masses. GJ-1 ($^{206}Pb/^{238}U$ 602.1 ± 0.7 Ma; Jackson et al. 2004) was used as primary standard for U–Pb ratios and NIST SRM 612 was used for quantification of element concentrations (U and Th). Stoichiometric SiO_2 = 32.8 wt% in zircon was used as internal standard. Plešovice ($^{206}Pb/^{238}U$ 337.13 ± 0.37 Ma; Sláma et al. 2008) was used as a secondary standard for accuracy and long-term reproducibility control. Population ages for Plešovice were within error of the accepted reference age in all sessions (Fig. S2 Online Resource 2). The long-term reproducibility of Plešovice $^{206}Pb/^{238}U$ dates was 1.4% (2 S.D., standard deviation) for a period of 17 months and on average ~ 2.0% (2 S.D.) for individual analytical days. U–Pb data were processed offline using the software Iolite 2.5 (Paton et al. 2010, 2011) and the data reduction scheme Visual ages (Petrus and Kamber 2012). Error propagation was carried out using Iolite (Paton et al. 2010). Only concordant (i.e. error ellipse intersects Concordia) dates are reported (Fig. S3 Online Resource 2), and no common Pb correction was applied. All U–Pb dates reported in this publication are $^{206}Pb/^{238}U$ dates. The term 'date' in this study refers to an individual U–Pb zircon spot analysis, while the term 'age' is used for a number of pooled dates, which are regarded as having geological significance. Errors on individual dates and isotope ratios are reported as 2 standard error (S.E.). U–Pb and trace element LA-ICP-MS analyses measure a 3D volume, while textural characterisation and spot selection were based on 2D CL-images. Mixing by accidentally drilling into relic cores and/or multiple rim generations at depth is a general concern. To minimise this risk we only targeted growth zones wide enough to fit our laser spot without the risk of drilling into other growth zones visible in CL-images. Furthermore, during data reduction we monitored and carefully evaluated each signal individually, using only flat signal parts and avoiding inclusions. Analyses that did not fulfil this criterion or showed obvious signs of mixing have been discarded.

Data reduction for trace element concentration was done with the MATLAB-based program SILLS 1.3.2 (Guillong et al. 2008). SRM 612 (primary standard) and SRM 610 (secondary standard) were used to standardise trace element data (reference values from Pearce et al. 1997 were used). Accuracy for trace elements with relatively high concentration is within ~ 5%, while trace elements close to detection limit have accuracy of ~ 10%.

Results

Regional metamorphism in metasediments from Val Strona di Omegna

Zircon textures

To study the internal textures of zircon by CL-images and make representative descriptions for each sample, we aimed to have at least 100 individual zircon grains per sample (Table 1); overall our study investigated 2576 zircon grains. Based on our observation, four types of core–rim proportions were distinguished in metapelitic zircon from Val Strona di Omegna, as schematically shown in Fig. 3a: *Type1* is dominated by a detrital core with a very narrow or no metamorphic rim; *Type2* shows a prominent detrital core with a variable (10–60 µm) metamorphic rim; *Type3* is dominated by the metamorphic rim with a small or relic core; *Type4* shows metamorphic zircon only, with no core visible.

Within metamorphic zircon, a sequence of texturally different metamorphic rims is distinguished based on their CL-appearance (Fig. 3b): from internal to external: *Rim1* is bright in CL, has an irregular shape and contains many

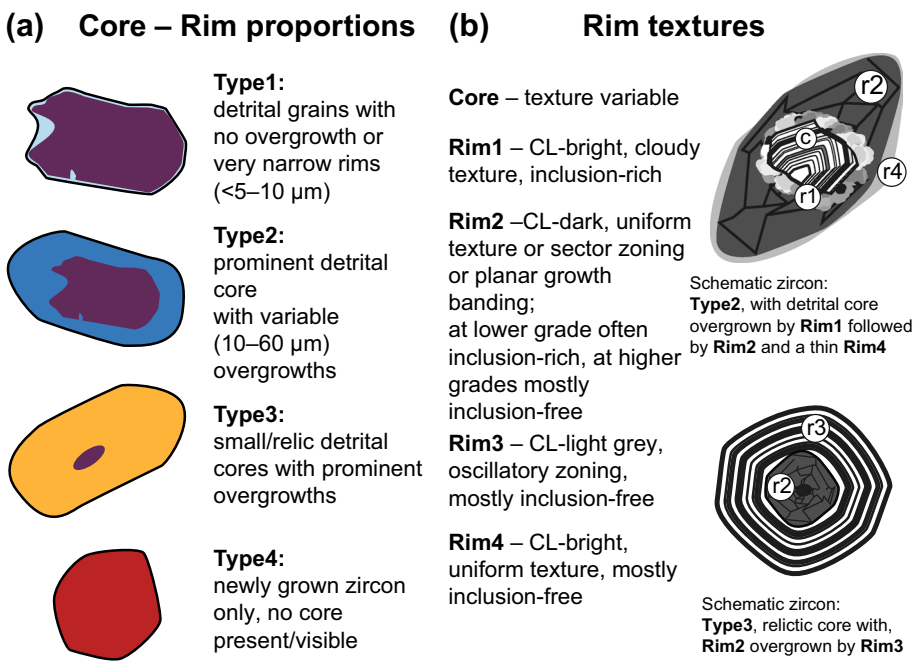

Fig. 3 Schematic sketches of zircon core–rim proportion types and internal rim textures. *c*, core; r1, *Rim1*; r2, *Rim2*; r3, *Rim3*; r4, *Rim4*

inclusions. *Rim2* is dark in CL, the internal texture is either uniform or shows sector zoning or growth banding or fir-tree zoning. *Rim3* displays oscillatory zoning and an intermediate grey CL-colour, and *Rim4* is bright and featureless in CL. Individual zircon grains rarely show all four types of rims, usually various subsets of these rims are observed (Fig. 4).

In mid-amphibolite facies metapelites, the examined zircon grains show an elongate or stubby crystal habit, commonly reflecting the shape of a detrital core. Towards the upper amphibolite and granulite facies, grains commonly show a 'soccer ball' shape, roundish with many crystal facets. In metapelite samples from Val Strona di Omegna, the proportion of preserved detrital or inherited core to metamorphic rim decreases with increasing metamorphic grade (Fig. 4). In the mid-amphibolite facies samples, *Type1* and *Type2* dominate the zircon population. In the upper amphibolite facies, *Type2* and *Type3* are most abundant, while in the granulite facies samples *Type3* and *Type4* predominate. With increasing grade, from mid-amphibolite facies towards upper amphibolite facies, *Rim1* increases in width, reaching its maximum thickness (up to 30 µm, Fig. 4) in sample IZ 422. Towards higher grade, *Rim1* becomes less prominent, and generally only a thin (< 5 µm) relic remains (Fig. 4, IZ 407, IZ 406 a, b, IZ 405). Overall, *Rim2* is the most abundant rim and it is observed across the mid-amphibolite to granulite facies. In the mid-amphibolite facies, *Rim2* is narrow (< 5 µm), whereas it starts to show significant width (> 30 µm) in the upper amphibolite facies (Fig. 4, IZ422). At upper amphibolite facies conditions, *Rim2* frequently is rich in sillimanite inclusions. *Rim3* (Fig. 4, IZ 406a, b) occurs only in leucosome-rich samples of the granulite facies, while the occurrence of *Rim4* (1–50 µm) is independent of metamorphic grade, though it is not present in every grain (Fig. 4).

Although abundant zircon grains were recovered from the metapsammites, the overall quality of the crystals was poor (i.e. broken grains, internal cracks or other forms of disturbance, Fig. 5). Independent of metamorphic grade, zircon grains are mostly dominated by detrital cores with narrow rims (< 5–10 µm). The granulite facies sample (IZ 424) shows substantial metamorphic rim growth (up to 50 µm). The same four rim types as for the metapelites could be identified (Fig. 5). *Rim1* is present predominantly in the amphibolite facies (IZ 417), *Rim2* is the most abundant rim type, *Rim3* occurs only in the granulite facies (IZ 424) and *Rim4* occurs independent of metamorphic grade (Fig. 5).

U–Pb zircon geochronology

An overview of U–Pb dates for each sample is shown in Table 2, individual analyses for each sample are listed in Online Resource 4 Tables S1 and S4. Both rock types (metapelite and metapsammite) will be described and discussed together according to their metamorphic grade. In samples from Val Strona di Omegna we analysed 169 detrital cores and 386 metamorphic rims (Table 2). Overall, the detrital core dates range from ~ 2640 to 352 Ma (Table 2), whereas the metamorphic rim analyses cover a range from 316 to 211 Ma (Table 2; Fig. 6; S9 Online Resource 3).

Mid-amphibolite facies: Metamorphic rims in sample IZ 410, IZ 417 and IZ 421 were too narrow to be analysed without the risk of accidentally mixing multiple rim generations;

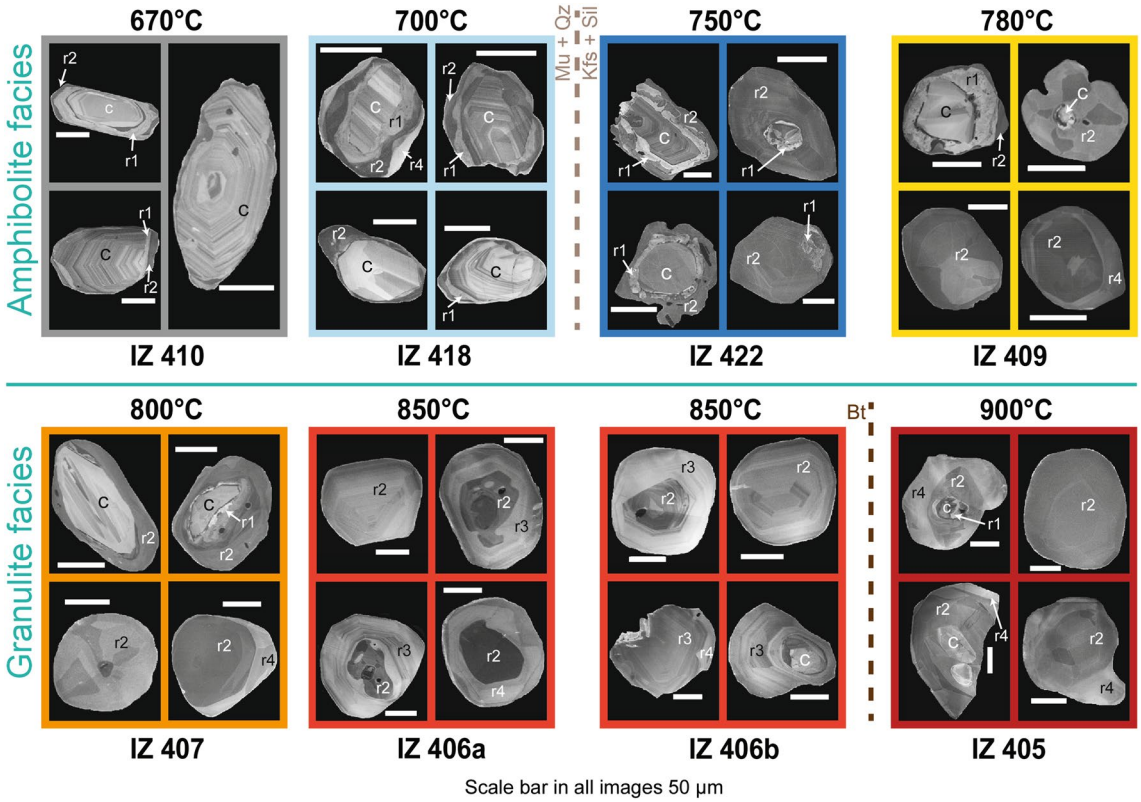

Fig. 4 Internal zircon textures from metapelites of Val Strona di Omegna. CL-images from zircon along the continuous metamorphic field gradient. In the lowest grade samples detrital cores dominate the internal zircon textures. With increasing metamorphic grade these detrital cores get resorbed, and new metamorphic zircon growths are wider. In the granulite facies samples, cores are only present as small relics. c, core; r1, *Rim1*; r2, *Rim2*; r3, *Rim3*; r4, *Rim4*

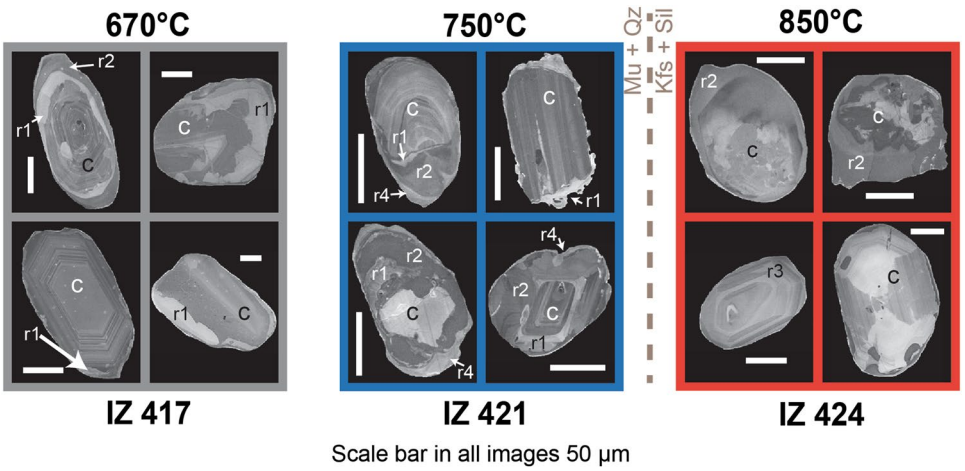

Fig. 5 Zircon from metapsammite in Val Strona di Omegna. CL-images with internal zircon textures; the internal textures are dominated by detrital cores. c, core; r1, *Rim1*; r2, *Rim2*; r3, *Rim3*; r4, *Rim4*

however, we suggest they are Permian in age by analogy with datable ones. The other mid-amphibolite facies samples (IZ 422 and IZ 418) show a narrow range of dates (Table 2; Fig. 6a): sample IZ 422 has a range of 288–276 Ma; IZ 418 yielded only two analyses (300 and 310 Ma) and is thus of limited significance. All obtained U–Pb dates from the mid-amphibolite facies were analysed in *Rim2* (Table S1 Online Resource 4).

Upper amphibolite facies: In the upper amphibolite facies, sample IZ 409 shows a range of Permian dates (291–254 Ma) that exceeds the spread expected form analytical uncertainty alone (Fig. 6b). Sample IZ 407, sampled close to the granulite facies transition, appears to show

Table 2 Overview of U–Pb ages, Th-, U- and Ti concentration for samples from the Ivrea Zone

Sample	Permian metamorphic dates								Detrital dates		
	# analyses	Max (Ma)	Min (Ma)	U (ppm)	Th (ppm)	Th/U	Ti (ppm)	Ti-T (°C)	# of detrital core analyses	Max (Ma)	Min (Ma)
Val Strona di Omegna											
IZ 410	–	–	–	–	–	–	–	–	44	2565 ± 54	535 ± 15
IZ 417	–	–	–	–	–	–	–	–	*12*	*1996 ± 63*	*436 ± 12*
IZ 418	2	309 ± 5	301 ± 19	1255–1496	5–6	0.004	0.6*–0.7*	540–553	26	2640 ± 140	558 ± 9
IZ 421	–	–	–	–	–	–	–	–	*22*	*916 ± 42*	*445 ± 21*
IZ 422	15	288 ± 8	276 ± 10	639–1050	4–8	0.006–0.009	1.3*–2.9	588–624	19	2672 ± 61	456 ± 17
IZ 409	66	291 ± 16	254 ± 6	281–1192	6–148	0.009–0.526	2.0–6.5	618–705	15	2510 ± 130	508 ± 19
IZ 407	23	316 ± 16	264 ± 12	120–2972	13–86	0.010–0.715	6.7–15.3	707–780	14	1968 ± 85	352 ± 16
IZ 424	*6*	*303 ± 14*	*265 ± 12*	*220–1248*	*3–50*	*0.002–0.113*	*9.2–52.3*	*733–911*	*13*	*746 ± 38*	*365 ± 8*
IZ 406a	73	297 ± 17	231 ± 12	63–1110	14–302	0.035–1.470	6.9–20.4	709–808	–	–	–
IZ 406b	93	308 ± 10	240 ± 9	54–1131	6–400	0.008–1.036	2.4–19.2	629–802	–	–	–
IZ 405	108	299 ± 11	211 ± 6	240–2817	4–826	0.002–0.847	4.8–38.7	680–876	4	1933 ± 57	354 ± 17
Val Sesia											
IZ 416	2	281 ± 8	269 ± 8	1072–1593	15–21	0.013–0.014	3.0–3.4	645–653	4	961 ± 35	586 ± 18
IZ 415	14	290 ± 8	269 ± 9	302–743	2–7	0.005–0.011	1.6*–4.1	604–668	2	660 ± 22	595 ± 16
IZ 411	*2*	*277 ± 10*	*271 ± 9*	*434–911*	*6–9*	*0.010–0.014*	*4.6*	*678*	*50*	*1795 ± 82*	*412 ± 21*
IZ 412	30	312 ± 22	265 ± 9	273–2012	8–335	0.009–0.374	1.0*–20.4	570–808	2	626 ± 45	449 ± 14

Italic: metapsammite samples

*Value close to detection limit

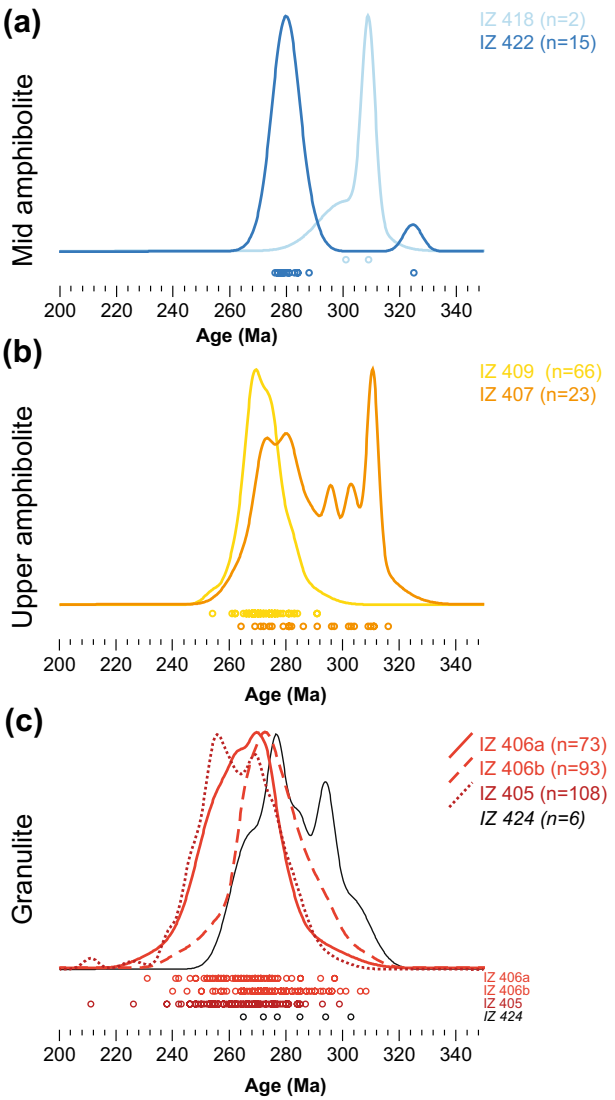

Fig. 6 Probability density plots of metamorphic U–Pb zircon ages from metapelites in Val Strona di Omegna. Sample IZ 406 consists of IZ 406a paleosome (solid line) and IZ 406b leucosome (dashed line). Circles below the probability density curve represent individual dates, plotted without their analytical error for simplicity

two age populations (see probability density plots (PDP); Fig. 6b) with an overall range of U–Pb dates from 316 to 264 Ma. Except for two spots in IZ 407, which were analysed in *Rim3* and *Rim4*, all U–Pb dates in the upper amphibolite facies were measured in *Rim2* (Table S1 Online Resource 4). The two analyses in *Rim3* and *Rim 4* are within error of the other ages in sample IZ 407.

Granulite facies: Samples from the granulite facies show a wide spread in U–Pb dates (Fig. 6c). Zircon rims in the metapsammite IZ 424 yielded a range of dates from 303 Ma to 256 Ma. Two distinct portions of metapelite IZ 406 were analysed separately; the melanosome (IZ 406a) and the leucosome (IZ 406b) show a similarly large spread of dates (Fig. 6c). Sample IZ 406a yields a range of dates from 280 Ma to 250 Ma while sample IZ 406b yields a range between ~300 and ~250 Ma. The highest grade sample IZ 405 shows a broad peak in the probability density plot (Fig. 6c), with U–Pb dates ranging from ~290 to 240 Ma. U–Pb dates were obtained for *Rim2, Rim3* and *Rim4*; however, no relationship between rim type and metamorphic dates has emerged (Fig. 8; S6a, b Online Resource 3; Table S1 Online Resource 4).

Trace element geochemistry of metamorphic zircon rims

Th/U ratios, Ti-in-zircon concentration as well as other trace elements (Hf, P, Y, REE) were measured for the same growth zones, close to the spots used for U–Pb dates. Table 2 gives an overview of the Th, U, Ti concentrations and the Th/U ratio for each sample. Individual analyses of trace elements are listed in Table S3 and S5 Online Resource 4. Trace element data are presented for metamorphic zircon. Since no systematic differences were evident between the data from different rim texture types defined above, the trace element results are described together below.

Metamorphic zircon rims in mid-amphibolite facies samples (IZ 418, IZ 422) are characterised by Th/U < 0.01 (Fig. 7a). In the upper amphibolite facies, Th/U ratios range from ~0.01 to 0.1 in most samples (IZ 409, IZ 407). Granulite facies samples show mostly high Th/U ratios between 0.1 and 1.0, but in samples IZ 405 the Th/U ratios cover a wide range (0.002–0.847, Table 2). In samples with scattered U–Pb dates we observe no correlation between Th/U ratios and U–Pb dates (Fig. 8a), except in sample IZ 407 where we see an increase in Th/U ratio with decreasing dates (Fig. 7c). Ti concentrations in metamorphic zircon rims are low and close to detection limit (~0.5–3 ppm) in the mid-amphibolite facies samples (Fig. 7d). In the upper amphibolite and granulite facies, minimum values are around 2 ppm (close to detection limit), while the maximum concentration (up to 38 ppm) and the scatter in the data increase towards higher grade (Fig. 7b; Table 2). Metamorphic zircon in the granulite facies samples yield a large spread in Ti concentration, with no correlation to their respective U–Pb dates (Figs. 7d, 8b). To calculate Ti-in-zircon temperatures, the calibration of Watson et al. (2006) was used, assuming a Ti activity of $a_{TiO2}=1$ (see Discussion for more details). Ti-in-zircon temperatures (Fig. 7b; Table 2) in the mid-amphibolite facies range from 540 to 620 °C. In the upper amphibolite facies, zircon yielded temperatures in the range of 620–780 °C, and in the granulite facies of 630–880 °C. While we observed an increase of scatter in Th/U ratios and in Ti concentration for granulite facies zircon, there is a correlation between these two variables (Fig. 8c, d). Generally speaking, independent of metamorphic grade of the sample, all zircon with low Ti concentration also have low(er) Th/U ratios (Fig. 8c, d).

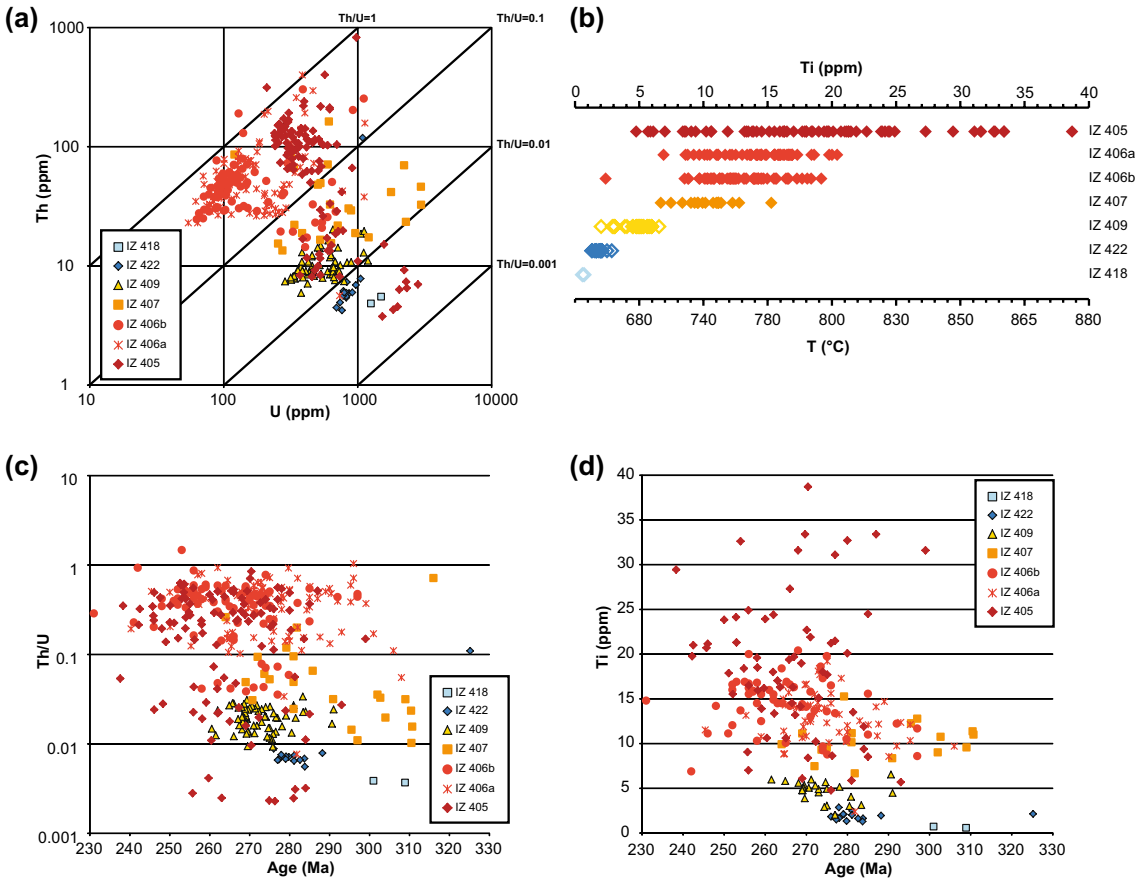

Fig. 7 Zircon trace element data from metapelites in Val Strona di Omegna. **a** Th vs. U concentration, **b** Ti-in-zircon concentration and temperatures, temperatures are calculated assuming $a_{SiO2} = a_{TiO2} = 1$. Open symbols indicate samples where rutile is not observed, so temperatures are minimum estimates. **c** Th/U ratio vs. U–Pb date **d** Ti-in-zircon concentration vs. U–Pb date. Symbols with black rim indicate samples where rutile is not present in the peak assemblage

This overall trend is also observed in sample IZ 405 with the biggest spread in Th/U and Ti concentration (Fig. 8c; Fig. S6b Online Resource 3).

Metamorphic zircon rims are characterised by REE patterns depleted in LREE with respect to HREE; chondrite-normalised (McDonough and Sun 1995) REE plots are shown in Fig. S4 Online Resource 3. A strong negative Eu anomaly[1] and slightly positive HREE patterns are seen in the mid-amphibolite facies zircon samples. In the upper amphibolite facies, the Eu anomaly (Eu/Eu* 0.03–0.27) is more variable, while HREE slopes are overall flat in sample IZ 409 (Lu_N/Gd_N 0.7–2.8) and flat to slightly negative in sample IZ 407 (Lu_N/Gd_N 0.1–5.2). In sample IZ 407 we observe a decrease in Hf and Yb concentration from older to younger ages (Fig. S5 Online Resource 3). The range in Eu anomaly in granulite facies samples is similar as at the upper amphibolite facies (Eu/Eu* 0.03–0.29), but the HREE patterns show much variability in the granulite facies, ranging from negative to positive (Lu_N/Gd_N 0.03–10.17). Sample IZ 405 shows large variability in REE composition, but a significant proportion of analyses show low HREE concentrations that are not observed in other samples.

Contact zone with Mafic Complex (Val Sesia)

In Val Sesia a narrow sliver of the Kinzigite Formation is exposed next to the Mafic Complex (Fig. 1), far less extensive here than in Val Strona di Omegna. The metamorphic grade of the country rocks in Val Sesia is comparable with the area around the Kfs/Ms isograd in Val Strona di Omegna (Redler et al. 2012). Samples were collected at various distances from the intrusive contact to the Mafic Complex (see Fig. 9a). Sample IZ 411 and IZ 412 were selected next to the intrusive contact, while samples IZ 415 and IZ 416 were taken some 500 m away from that contact (Fig. 9a). As in Val Strona di Omegna, a limited range of bulk rock compositions (metapelite, metapsammite, leucosome) was studied

[1] $Eu/Eu^* = [Eu_N/\sqrt{(Sm_N \times Gd_N)}]$.

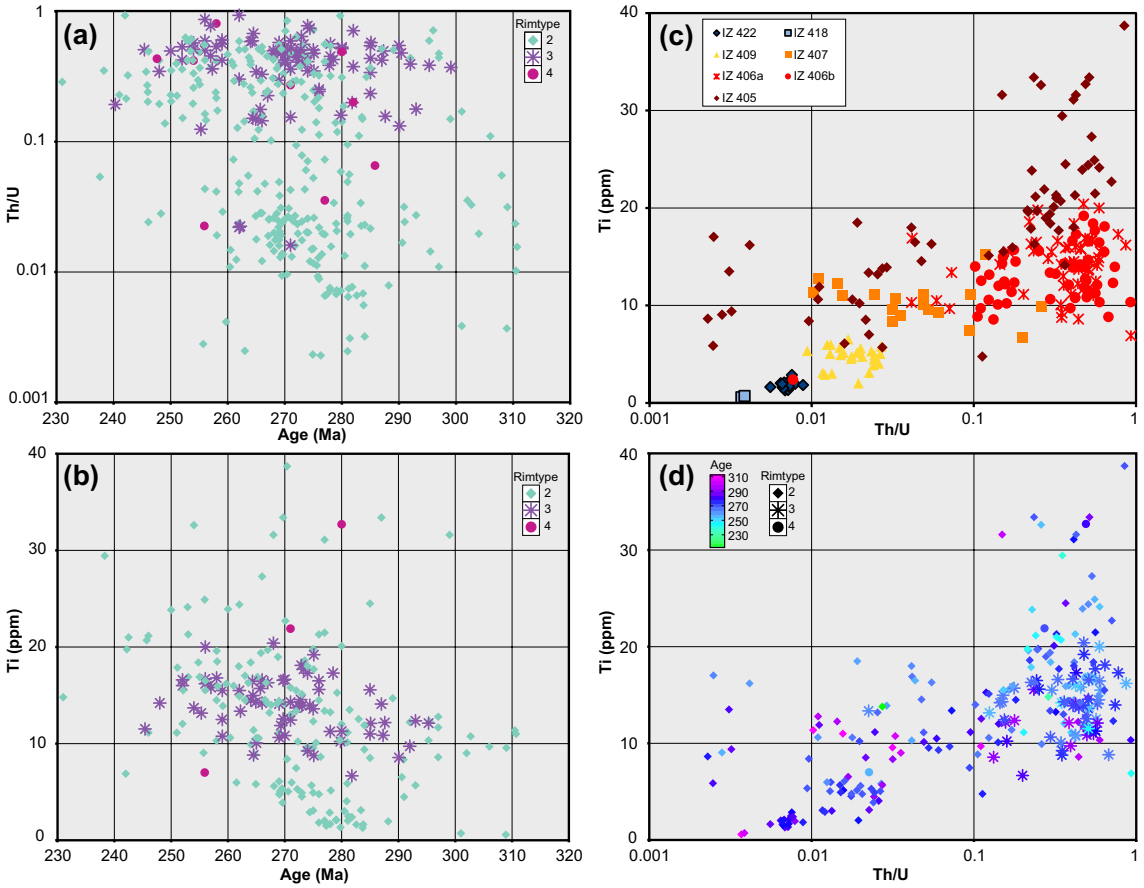

Fig. 8 Zircon rim type and trace element data plots for metapelites from Val Strona di Omegna. **a** Th/U ratio vs. U–Pb date distinguishing between different rim types. **b** Ti concentration vs. U–Pb date distinguishing between different rim types. **c** Ti concentration vs. Th/U ratios plotted according to sample (and metamorphic grade). **d** Ti concentration vs. Th/U ratios plotted with their U–Pb date (colour) and rim type (symbols)

to investigate the bulk rock composition influence in the behaviour of zircon.

Zircon textures

The metapelitic samples IZ 415 and IZ 416 from Val Sesia show internal zircon textures similar to those from the upper amphibolite facies (IZ 422 and IZ 409) in Val Strona (Fig. 9b, c.f. Fig. 4). In sample IZ 416 well-developed *Rim1* and *Rim2* overgrow detrital cores, while in IZ 415 *Rim1* is rarely preserved and overgrown by up to 50 µm *Rim2* (Fig. 9b). In both samples detrital cores show features of partial resorption. Sample IZ 412 is a garnet-rich leucosome that retains abundant evidence of a detrital origin of many zircon cores. The rim is either uniformly dark in CL or shows oscillatory zoning. Several grains show evidence for inward migrating reaction fronts (see Fig. 9b). Zircons in metapsammite sample IZ 411 are dominated by detrital cores with a narrow metamorphic *Rim2* (Fig. 9b). Some metamorphic rims show zoning that curves inwards, and detrital cores show evidence of cloudy and/or turbulent overprinting of previously developed textures (Fig. 9b).

U–Pb zircon geochronology

Fifty-eight detrital cores were analysed, yielding dates from 1795 to 412 Ma, while 48 analyses of metamorphic rims yield a range of dates from 312 Ma to 265 Ma (Fig. 9c; Table 2; Table S2 Online Resource 4). In metapelite IZ 415, zircon *Rim2* has a range of 290–269 Ma; the metamorphic rim in sample IZ 412 defines a range from 312 to 265 Ma. Owing to the overall narrow width (5–30 µm) of metamorphic rims, few zircons were analysed in IZ 411 and IZ 416. The dates obtained are in agreement with those from the other Val Sesia samples in our study.

Metamorphic zircon trace element geochemistry

Th/U ratios in Permian zircon range from 0.005 to 0.014, with the exception of zircons in sample IZ 412 (Th/U = 0.009

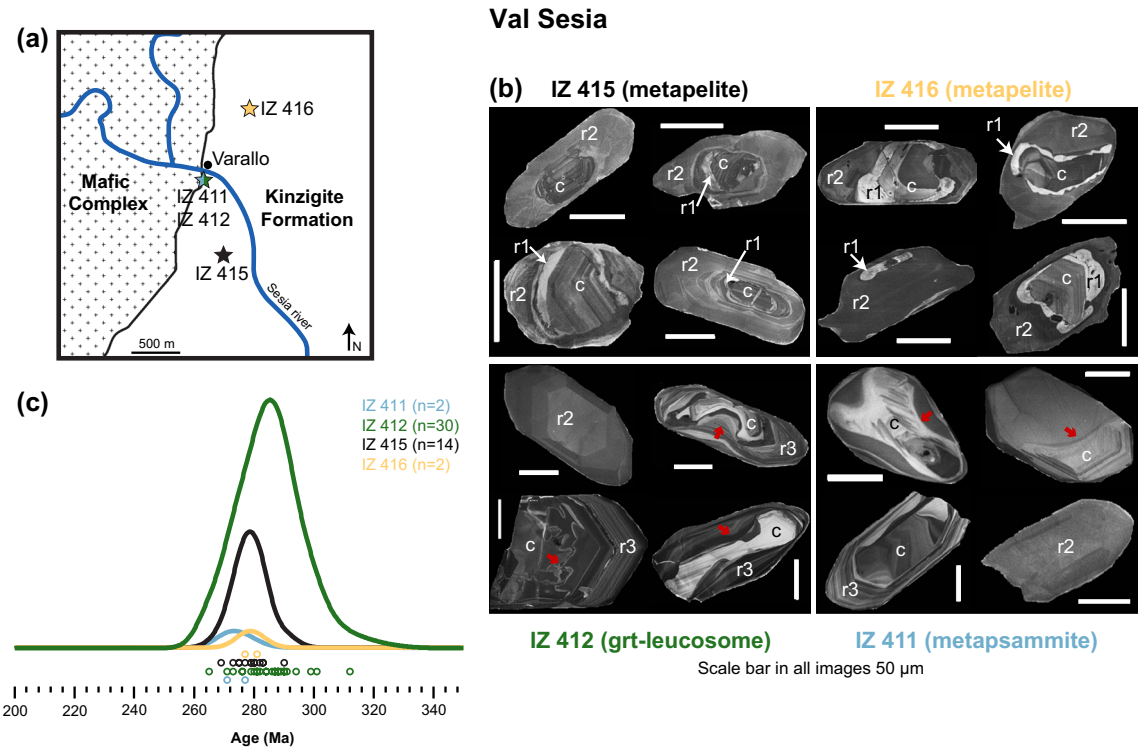

Fig. 9 Zircon from Val Sesia samples. **a** Simplified geological map of the sample area in Val Sesia with stars indicating the samples localities at different distances from the Mafic Complex. **b** CL-images of zircon from Val Sesia. Samples IZ 411 and IZ 412 show strong resorption of internal zones as well as inward migrating reaction fronts (small arrows). Samples IZ 415 and IZ IZ 416 show detrital cores followed by a *Rim1* and *Rim2*, comparable to the upper amphibolite facies sample IZ 422 from Val Strona di Omegna (Fig. 4). c, core; r1, *Rim1*; r2, *Rim2*; r3, *Rim3*; r4, *Rim4*. **c** Probability density plot of U–Pb zircon ages from Val Sesia

up to 0.374, Table 2; Table S3 Online Resource 4), Ti-in-zircon concentration for the Permian metamorphic rim range from 1 to 20 ppm (T = 570–810 °C); however, in most samples values are below 4 ppm, translating to temperatures of ~ 600–670 °C (Table 2). REE element patterns of Permian zircon are steep (Gd_N/Lu_N=3–111) and show a negative Eu anomaly (Eu/Eu* 0.04–0.59).

Discussion

CL-images of zircon textures in metapelites from Val Strona di Omegna show that detrital grains/cores were progressively resorbed with increasing metamorphic grade, whereas new metamorphic zircon grew (Fig. 4). Although *Rim2* at upper amphibolite facies conditions shows discrete age peaks and uniform trace element compositions (Figs. 6, 7, 8), towards higher grades the scatter in the zircon U–Pb dates increases significantly, as do the Th/U ratio and Ti concentrations (Figs. 7, 8). The chemical complexity of the zircons in individual samples, especially those in the granulite facies, indicates additional processes compared to those operating at lower metamorphic grade.

Evolution of zircon along the high-grade metamorphic field gradient

Zircon textures

Core–rim proportions in zircon from metapelites evolve continuously from mid-amphibolite facies (dominated by detrital core) to granulite facies (dominated by metamorphic rim) (Fig. 4). Previous studies have related such observations to the increasing degree of partial melting leading to resorption of detrital grains into the melt, which ultimately resulted in the growth of a thicker rim (e.g. Rubatto et al. 2001; Kelsey et al. 2008; Yakymchuk and Brown 2014).

According to our observations, we suggest that the four types of metamorphic rim textures recognised in zircon (Fig. 4) can be explained by different growth environments and/or mechanisms:

- *Rim1* and detrital cores, with bright-CL intensity, numerous inclusions, and cloudy zoning have the characteristics of zircon grown by a fluid-assisted dissolution–reprecipitation process (e.g. Tomaschek et al. 2003; Geisler et al. 2007; Vonlanthen et al. 2012; Rubatto 2017). Ages

for *Rim1* could not be obtained due to their narrowness, generally very low U-contents and abundant inclusions.
- *Rim2* has textural features typical for anatectic growth at HT conditions in the presence of a melt, i.e. dark-CL emission (U-rich), uniform in CL-appearance or sector zoned (e.g. Vavra et al. 1996, 1999; Schaltegger et al. 1999; Rubatto and Gebauer 2000; Corfu et al. 2003). This rim type is the most abundant and occurs in amphibolite facies samples as well as samples of restite or melanosome at granulite facies.
- *Rim3* only occurs in leucosome-rich granulite facies samples (Fig. 4, IZ 406 a, b). Its fine-scale oscillatory zoning or planar growth banding suggests crystallisation from an anatectic melt (e.g. Hoskin 2000; Corfu et al. 2003).
- *Rim4* shows features typical for late-stage fluid-induced recrystallisation, as reported by Vavra et al. (1999). The enhanced CL-emission in this rim type may be related to a purification process (trace element rejection) in the zircon crystal structure (e.g. Schaltegger et al. 1999; Vonlanthen et al. 2012).

Zircon from metapsammitic samples shows much less change with metamorphic grade. The zircon textures (Fig. 5; e.g. blurred zoning, 'ghost' zoning, convolute zoning, or inwards curved recrystallisation fronts) are typical features for solid-state recrystallisation, as described by Hoskin and Black (2000). Metapelites and metapsammites experienced the same *P–T* path (Redler et al. 2012), and both contained abundant detrital zircon in their precursor, but during metamorphism zircon evolved differently. In metapsammites (Fig. 5), resorption of cores and growth of new metamorphic rims were limited, as compared to metapelites (Fig. 4), indicating that the presence of a fluid or melt is a decisive factor, as shown by other studies (e.g. Rubatto et al. 2006; Kelsey et al. 2008).

Zircon geochronology and geochemistry

The U–Pb zircon dates from metasediments range between ~ 316 and 240 Ma, a spread of > 60 Myr. In the mid-amphibolite facies sample, metamorphic rims were too thin (5–30 µm) to be dated by LA-ICP-MS, hence it was not possible to confirm their age. The two upper amphibolite facies samples in Val Strona di Omegna and the samples from Val Sesia that represent similar upper amphibolite facies grade, each have a single, well-defined age generation, obtained in *Rim2*, with homogenous trace element patterns (Figs. 6, 7, 8, S4–S6a Online Resource 3).

Close to the upper amphibolite/granulite facies transition, two age generations are present, and these are distinguished by Th/U ratios (Fig. 7c) as well. In the granulite facies samples, U–Pb zircon dates scatter broadly over > 40 Myr (Fig. 6). Similarly broad age ranges in granulite facies zircon population have been described in several studies from other terrains (e.g. Rubatto et al. 2001; Diener et al. 2013). Despite the scatter of dates in the granulite facies samples, a trend (Fig. 6) towards on average younger ages (c. 260 Ma) is visible in our samples, compared to those in the upper amphibolite facies. Younger ages in deeper crustal levels suggest either (1) later onset of zircon crystallisation or (2) disturbance of zircon at high-grade conditions. Given the broad scatter in dates, it seems unlikely that the data can be simply explained by later onset of zircon crystallisation. As suggested by other studies (e.g. Taylor et al. 2016), a combination of disturbance and episodic or continuous growth could be a more plausible reason for the scatter. In the present case, Pb loss could result in a spread of dates along Concordia instead of apparently discordant ellipses due to the relatively young metamorphic ages. While we cannot completely rule out this possibility, we see no correlation between U (+ Th) and U–Pb dates in any of our samples; therefore, we do not consider this to have a major effect on our data or the observed decoupling.

Except for five outliers, mid- and upper amphibolite facies samples generally have Th/U ratios < 0.1 (Fig. 7a), while granulite facies samples mostly show Th/U ratios > 0.1 (Fig. 7a). This reflects well-documented trends, i.e. Th/U ratios < 0.1 in metamorphic zircon (Rubatto and Gebauer 2000). However, in some granulite facies (> 900 °C) and (U) HT terranes (e.g. Rogaland: Möller et al. 2003; Napier Complex: Kelly and Harley 2005; Eastern Ghats belt: Korhonen et al. 2013), metamorphic zircon with Th/U ratios > 0.1 are well known. The trend towards higher Th/U ratios in zircon with increasing metamorphic grade reflects both an increase in Th and a decrease in U concentrations. Th and U availability are controlled by the abundance of other major or accessory phases and their partitioning with zircon. However, our present data are from zircon grain separates, so the textural context required to further investigate this is lacking.

Ti-in-zircon temperatures (540–640 °C) for amphibolite facies samples (IZ 418, IZ 422) are considered minimum values, due to lowered TiO_2 activity in the absence of rutile (e.g. Watson et al. 2006). In the other studied samples, rutile is abundantly present as large grains (~ 30–500 µm), and temperatures are considered to relate to zircon growth between 620 and 880 °C. Ti-in-zircon temperatures (Table 2) are clearly lower than the inferred peak temperature (Table 1) for the Ivrea Zone (up to 950 °C, Luvizotto and Zack 2009; Ewing et al. 2013), such discrepancy has been observed in other studies as well (e.g. Baldwin et al. 2007; Ewing et al. 2013). For cases with such discrepancy it has been proposed that Ti-in-zircon temperatures do represent zircon growth, which occurred below peak temperature (e.g. Roberts and Finger 1997).

To explain the observed increase in maximum Ti concentration with increasing metamorphic grade and the increased

scatter in granulite facies samples (Fig. 7b, d), we consider (1) zircon growth in a non-buffered system, or (2) zircon growth over a range of temperatures. Looking at these possibilities in turn: (1) in quartz-bearing rocks, such as metapelites, SiO_2 was surely buffered (a_{SiO2}=1). While rutile is present in the mineral assemblages of all but two samples, it is possible that the TiO_2 activity (relative to rutile) was lower at the time and/or in the reaction volume in which zircon grew; if so, the calculated temperatures represent minima. (2) If the system was buffered at a_i=1 for both SiO_2 and TiO_2, the calculated Ti-temperatures delimit the interval in which zircon actually grew. This may imply zircon growth at different stages along the same metamorphic path (e.g. prograde, peak and retrograde). The range of Ti-in-zircon concentrations in our highest grade samples is remarkably large (4–38 ppm; 680–880 °C); however, there is no correlation between Ti concentration and U–Pb ages, limiting, in our samples, the use of the Ti-in-zircon thermometer as a petrochronological tool. Furthermore, heterogeneous Ti distribution at sub-micron scale (e.g. Hofmann et al. 2009; Kusiak et al. 2013a, b) may cause a spread in the apparent Ti-in-zircon temperatures but, given the small extent (< 1 µm) of such patches, it remains unclear to what degree they might influence our trace element data (analyses made with a spot size of 32 µm).

In summary, our data show that in granulite facies zircon there is no correlation between U–Pb dates and internal textures, Th/U ratio, or Ti-in-zircon concentration (Fig. 8, S6a, b Online Resource 3); however, a positive correlation between Th/U ratio and Ti-in-zircon concentration has been identified (Fig. 8a, b). This correlation is observed when looking at all metapelitic samples from Val Strona di Omegna as well as in sample IZ 405 where the biggest spread in Th/U ratios and Ti concentration is observed (Fig. 8; S6a, b Online Resource 3). This possibly indicates that zircon grew at different stages along the *P–T* path of IZ 405, but owing to the decoupling of the U–Pb ages from Th/U ratios and Ti concentration such an interpretation is uncertain.

Heterogeneities between and within individual samples

Granulite facies samples are characterised by younger ages, higher Th/U ratios and Ti-in-zircon concentration, matched with a large scatter in the data (Figs. 6, 7). What caused the age difference between zircon in upper amphibolite and granulite facies samples? More specifically, how does the difference in age relate to the difference in metamorphic grade, and why are the data so scattered in the granulite facies? Did granulite facies samples experience several phases of zircon growth, while upper amphibolite facies samples only experienced one? Is zircon (more) affected by disturbance at granulite facies conditions?

We suggest that possible explanations for the scattered granulite facies zircon data fall into two main categories: (1) prolonged or episodic growth of zircon, and (2) isotopic or geochemical disturbance of (primary) zircon during a protracted HT history (post-crystallisation).

- In granulite facies samples we observe no trends between U–Pb dates, Th/U ratios, and Ti-in-zircon temperatures (Fig. 7c, d). However, there is a trend between Th/U ratios and Ti concentration, indicating zircon growth at different stages. While we cannot rule out that some of the observations in the granulite facies zircon population are the result of several growth episodes or of protracted growth during the prolonged HT metamorphism, such evidence has been obscured by subsequent processes that affected zircon or may be obscured due to analytical limitations in our data.
- Isotopic and/or geochemical disturbance of zircon by various mechanisms—at times occurring in combination—has been suggested by other authors (e.g. Vavra et al. 1999; Ewing et al. 2013). Previous studies have found that amphibolite facies samples are less prone to disturbance than granulite facies samples, but no particular process has been accepted to account for this phenomenon (e.g. Schiøtte et al. 1989; Williams 1992; Vavra et al. 1999). In a previous study Vavra et al. (1999) interpreted the spread of granulite facies zircon dates in the Ivrea Zone as the result of zoning-controlled alteration (ZCA). ZCA can cause rejuvenation in a process that preferentially occurs along primary textural features such as sector boundaries, inclusions or growth banding. While some grains in our granulite facies sample do show textures similar to those described by Vavra et al. (1999), we found no correlation between younger dates and these textures.

Furthermore, the strongest heterogeneity is evident in the highest grade sample IZ 405 (Fig. 10). We observe grains that show the same date (262 ± 5 and 262 ± 9 Ma), but clearly different textures (oscillatory zoning and sector zoning, Fig. 10a), as well as the reverse, i.e. the same texture (fir-tree zoning) but different dates (265 ± 7 Ma and 242 ± 6 Ma, Fig. 10b). Similar observations also pertain to the date and Ti concentration (Fig. 10c, d), and to the Th/U ratio (Fig. 10e, f). These observations clearly indicate decoupling of zircon chemical and isotopic signatures in the granulite facies samples from Val Strona di Omegna.

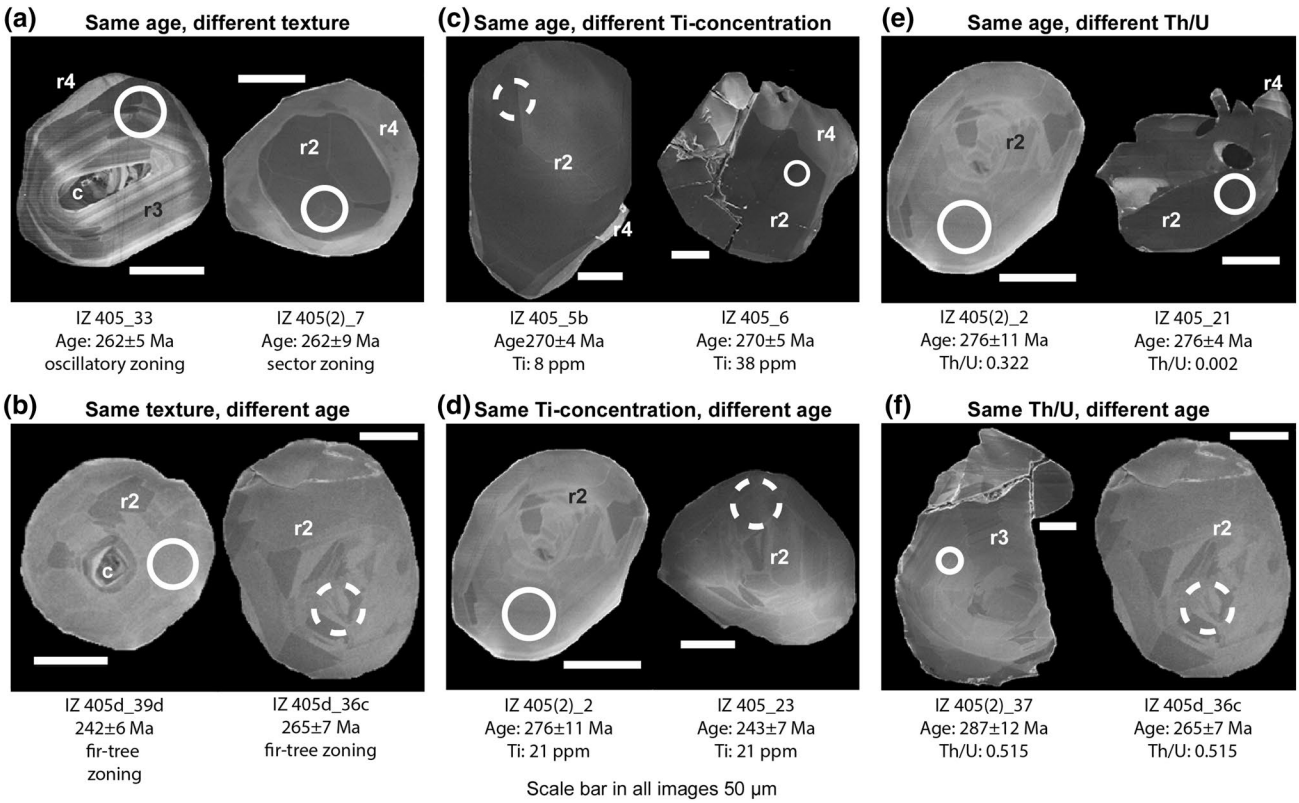

Fig. 10 Individual zircon grains from granulite facies sample IZ 405 showing the decoupling of zircon texture, Th/U ratios, and Ti concentration from U–Pb dates. Solid circles LA-ICP-MS spot 32 µm; dashed circles LA-ICP-MS spot 44 µm

Based on our data, we exclude several potential processes as the cause for the observed decoupling of zircon dates from trace element compositions:

1. Given the low U concentration (< 1000 ppm) in granulite facies zircon and relatively short accumulation time (< 300 Ma), metamictisation and annealing of metamict domains are not among the possible disturbance mechanisms. In fact, no textures characteristic of metamict zircon—such as suppressed CL (Nasdala et al. 2002)—have been observed in any of our samples. The average α-doses calculated for zircons from our study (see Table S1 Online Resource 4) are 0.4×10^{15} α/mg, clearly below the first percolation point (Stage 1: 2.2×10^{15} α/mg; Pidgeon 2014) of radiation damage. We also do not observe any correlation between U–Pb dates and α-dose (see Fig. S7 Online Resource 3).
2. Fluid alteration can be excluded for *Rim2* and *Rim 3* in the majority of our samples from Val Strona di Omegna, since characteristic CL-textures are lacking, such as bright-CL domains, inward-penetrating reaction fronts or convolute zoning (e.g. Vonlanthen et al. 2012). *Rim1, Rim4*, and some detrital cores may have been affected by fluid alteration, based on their CL-appearance, but apart from that textural evidence, the respective geochronological and geochemical data are inconclusive. The majority of our data showing decoupling were obtained in *Rim2* or *Rim3*, where CL-textures are not disturbed.
3. Crystal plastic deformation is unlikely to be responsible for the bulk of our observations. Element redistribution under dry conditions without a chemical or structural sink (Piazolo et al. 2016) usually occur on the sub-micrometre scale (e.g. Valley et al. 2014) and are unlikely to have a dominant influence on our LA-ICP-MS data obtained with spot sizes of 44 to 32 µm. Sample IZ 407, taken inside a shear zone, is the only sample for which we observe a trend between U–Pb dates and geochemical data (Fig. 7 and Fig. S5 Online Resource 3).

The more intense thermal imprint (higher *T* and longer duration) experienced by the granulite facies samples remains a most likely factor responsible for the observed decoupling. Similar propositions have been put forward by other studies that reported decoupling of zircon characteristics (e.g. Flowers et al. 2010). Decoupling may be explained by different behaviour and retention of certain elements in the zircon structure. In particular, the contrasting fit and

diffusion behaviour of U and Pb in the zircon crystal lattice has been proposed as a possible cause for partial resetting of U–Pb ages (e.g. Cherniak and Watson 2003; Hoskin and Schaltegger 2003; Harley et al. 2007; Rubatto 2017). Rubatto and Gebauer (2000) reported that internal zircon textures shown by CL-images are mostly caused by trace elements such as Dy, Gd, Tb and U, so the preservation of CL-structures does not indicate preservation of the U–Pb growth age (Cherniak and Watson 2000).

Experimental results (Cherniak and Watson 2000) show that at ca. 750 °C it would take several billion years for a crystalline zircon with 10 µm radius to lose 1% of its lead. However, at 900 °C the same size zircon can lose more than 25% of its Pb in 1 million years or 50% in 10 million years. The highest grade samples in the Ivrea Zone experienced temperatures above 900 °C, the duration of these HT conditions remains uncertain despite many studies. While it seems possible that volume diffusion of Pb could be a cause for the observed decoupling, it would take further investigations (e.g. systematic in situ Pb profiling around zircon grains that show decoupling) to confirm its effectiveness on the observed length and timescale.

Other trace elements such as Ti or Th are considered similarly compatible in zircon as U, i.e. more unlikely to be disturbed than Pb (e.g. Hoskin and Schaltegger 2003). Patchy Pb and Ti distribution has been reported from (U)HT zircon, but in the case of Ti it remains unclear how common this is in (U)HT zircon and whether it is a primary or secondary feature (Kusiak et al. 2013a, b; Valley et al. 2014; Whitehouse et al. 2014). In the case of Pb, a study by Valley et al. (2014) showed that in their case, at the micrometre scale spots typically used in SIMS (or LA-ICP-MS) analysis, Pb nanoclusters did not have an influence on their ages. By contrast, Kusiak et al. (2013a, b) and Regis et al. (2017) reported that $^{207}Pb/^{206}Pb$ ages measured with ~ 20 µm SIMS spots were affected by Pb heterogeneity in their samples. Without investigating the Pb distribution and heterogeneity, one cannot be sure whether patchy Pb distribution caused the observed decoupling.

In our samples, given the observed correlation between Th/U ratios and Ti-in-zircon concentration, we surmise that the patterns observed in the Ti contents and Th/U ratios do reflect different growth periods, but that the U–Pb dates appear to have been disturbed. However, the detailed mechanisms responsible remain speculative until further investigations are made.

Similar decoupling between zircon ages and textures or Pb mobility in granulite facies zircon have been found in other areas, e.g. the Tasiuyak Gneiss, Labrador (e.g. McFarlane et al. 2005), in the western Canadian shield (Flowers et al. 2010), the Napier Complex, Antarctica (e.g. Kusiak et al. 2013a, b), the Kerala Khondalite Belt, South India (Whitehouse et al. 2014), and the Snowbird Tectonic Zone, Canada (Regis et al. 2017). All of these studies were conducted on Proterozoic rocks, whereas our study concerns granulite facies samples from the late Palaeozoic. Although the mechanism for disturbance is not known, high temperatures seem to be an essential factor, for decoupling of zircon characteristics is observed in granulite facies (> 850 °C) or UHT samples only.

Implications for the interpretation of the metamorphic evolution in the central Ivrea Zone

Our study demonstrates that parts of the lower Ivrea Zone experienced an extended period (~ 60 Myr) of HT metamorphism during the late Carboniferous to Permian times, as suggested by other studies (e.g. Vavra et al. 1999; Peressini et al. 2007; Ewing et al. 2013). Our survey of U–Pb zircon and monazite ages for metasedimentary samples from the different localities in the Ivrea Zone indicates that the main range of preserved metamorphic ages in the Kinzigite Formation and paragneiss-bearing belt is 280–260 Ma (Fig. S9 Online Resource 3). In Val Strona di Omegna, amphibolite facies samples show two narrowly constrained metamorphic age peaks in the Permian, at 280 ± 2 Ma and 272 ± 1 Ma, while the granulite facies samples span a wide range from 300 to 240 Ma. A previously reported U–Pb zircon metamorphic age at 316 ± 3 Ma (Ewing et al. 2013) has not been confirmed to be of regional occurrence in the metapelites from the Kinzigite Formation. Whether this is owed to the local preservation or to isolated growth of this age generation remains unclear. Our ages from amphibolite facies samples are within error of the 276 ± 4 Ma zircon recrystallisation age reported by Ewing et al. (2013). Our zircon ages for amphibolite facies samples are only slightly younger than the main intrusion phase of the Mafic Complex at 288 ± 4 Ma (Peressini et al. 2007) and might thus represent a contact metamorphic imprint. However, the studied samples from Val Sesia closest to the intrusion of the Mafic Complex have the same age (IZ 415; 278 ± 3 Ma) as the samples from Val Strona di Omegna. If indeed a contact metamorphic event was responsible for the younger growth generation of amphibolite facies zircon, we would expect to see the age to depend on the distance from the intrusion contact. This is not observed.

In the northeastern and southwestern parts of the Ivrea Zone, some samples show an age generation < 220 Ma (Zanetti et al. 2013; Schaltegger et al. 2015; Langone et al. 2017) we have found no evidence for that in Val Strona di Omegna (Fig. S9 Online Resource 3).

The cause of the long-lasting regional HT conditions in this deep crustal section remains an important controversy. Petrological studies found convincing evidence that the HT metamorphic field gradient was established prior to

the intrusion of the Mafic Complex (e.g. Zingg et al. 1990; Barboza et al. 1999; Barboza and Bergantz 2000; Redler et al. 2012). The present study, together with literature data, indicates a duration of ~60 Myr for the HT conditions in the Kinzigite Formation (Vavra et al. 1999; Ewing et al. 2013). Thermal modelling of intrusion-related thermal disturbances contend that thermal anomalies usually subside after < 10 Myr, independent of crustal parameters used (e.g. Annen and Sparks 2002; Bodorkos et al. 2002). Therefore, the long duration (~60 Myr) of HT conditions in the Kinzigite Formation is unlikely to have been caused by any single intrusion such as the Mafic Complex. The thermal history in the Ivrea Zone requires additional heat sources to raise temperatures to granulite facies conditions and sustain them for some 60 Myr. Considering the tectonic situation of the Ivrea Zone during Permian times, i.e. incipient rifting at a passive margin (e.g. Handy et al. 1999), the most likely source for long-lasting heat input into the crust is asthenospheric upwelling of the mantle during crustal thinning (e.g. Schaltegger et al. 2002). The idea that Permian HT metamorphism in the Ivrea Zone was caused by a large-scale thermal anomaly involving the mantle is supported by the large spatial and temporal extent of the evolution: abundant evidence for Permian HT metamorphism and magmatism is found in Adria-derived units all along the Alpine chain (e.g. Hermann and Rubatto 2003; Schuster and Stüwe 2008; Kunz et al. 2018). The abundant Permian mafic and felsic intrusions (e.g. Monjoie et al. 2007; Peressini et al. 2007; Schaltegger and Brack 2007) together with a thermal input from the mantle account for the HT conditions in the lower and middle crust, as has been shown for other regions by thermal modelling (e.g. Bodorkos et al. 2002). We thus conclude that regional-scale Permian HT metamorphism in the Adriatic margin was caused by a combination of asthenospheric upwelling, magmatic underplating and magmatic bodies intruding to different crustal levels.

Conclusion

The present study is the first work reporting decoupling in young (~280 Ma) non-metamict (average α-dose 0.4×10^{15} α/mg) zircon from a HT (> 850 °C) metamorphic terrain. Decoupling has been previously described, but only for zircon from Proterozoic rocks, where it was noted in radiation-damaged areas of zircon grains and was tentatively linked to Pb mobility during (U)HT metamorphism.

Here we document the evolution of zircon chemistry and ages along the Val Strona di Omegna metamorphic gradient: two amphibolite facies samples (< 750–800 °C) show a metamorphic rim (*Rim2*) of homogenous trace element geochemistry and well-defined U–Pb age, respectively, of 280 ± 2 Ma and 272 ± 1 Ma. Zircon from the highest grade samples (> 850 °C) are affected by HT disturbance that caused decoupling of U–Pb dates from their trace element geochemistry, while preserving the correlation between trace element characteristics (Th/U ratios and Ti concentration). Such decoupling hampers the ability to link and interpret the observed scatter in these data to different stages along the metamorphic evolution of the samples. Details of the process(es) that caused this disturbance remain uncertain; since lower grade samples were not affected, HT processes are inferred. As the zircon characteristics in samples closest to this intrusive body in Val Sesia show no unusual scatter, these processes are not directly related to the intrusion of the Mafic Complex.

Acknowledgements We thank Pierre Lanari and Thomas Pettke for their support with LA-ICP-MS measurements and discussions, and Matthias Bächli, Rahel Baumann, and Remo Widmer for help with mineral separation. We acknowledge fruitful discussions with Tanya Ewing, Daniela Rubatto, and Clare Warren, constructive reviews by Antonio Langone, Richard Taylor, and Chris Yakymchuk, as well as research funding provided by the Swiss National Foundation (Project 200020-146175). We thank Steven Reddy for editorial handling.

References

Annen C, Sparks RS (2002) Effects of repetitive emplacement of basaltic intrusions on thermal evolution and melt generation in the crust. Earth Planet Sci Lett 203:937–955

Baldwin JA, Brown M, Schmitz MD (2007) First application of titanium-in-zircon thermometry to ultrahigh-temperature metamorphism. Geology 35:295–298

Barboza S, Bergantz G (2000) Metamorphism and anatexis in the Mafic Complex contact aureole, Ivrea Zone, Northern Italy. J Petrol 41:1307–1327

Barboza S, Bergantz G, Brown M (1999) Regional granulite facies metamorphism in the Ivrea zone: is the Mafic Complex the smoking gun or a red herring? Geology 27:447–450

Berckhemer H (1968) Topographie des "Ivrea-Körpers", abgeleitet aus seismischen und gravimetrischen Daten. German Research Group for Explosion Seismology. Schweiz Mineral Petrogr Mitt 48:235–246

Bertolani M (1959) La formazione basica 'Ivrea Verbano' e la sua posizione nel quadro geologico–petrografico della Bassa Valsesia e del Biellese. Periodico di Mineralogia 28:151–209

Bertolani M (1968) La petrografia della Valle Strona (Alpi Occidentali Italiane). Schweiz Mineral Petrogr Mitt 48:695–733

Bigi G, Carrozzo MT (1990) Structural model of Italy and gravity map. Consiglio Nazionale delle Ricerche (Italia) 114:3

Bingen B, Austrheim H, Whitehouse M (2001) Ilmenite as a source for zirconium during high-grade metamorphism? Textural Evidence from the Caledonides of Western Norway and implications for zircon geochronology. J Petrol 42:355–375

Bodorkos S, Sandiford M, Oliver NH, Cawood PA (2002) High-T, low-P metamorphism in the Palaeoproterozoic Halls Creek Orogen, northern Australia: the middle crustal response to a mantle—related transient thermal pulse. J Metamorph Geol 20:217–237

Boriani A, Sacchi R (1973) Geology of the junction between the Ivrea–Verbano and Strona–Ceneri zones (southern Alps). Memorie degli Istituti di Geologia e Mineralogia dell'Universita di Padova 28:1–35

Boriani A, Burlini L, Sacchi R (1990) The Cosatto-Mergozzo-Brissago Line and the Pogallo Line (Southern Alps, Northern Italy) and their relationships with the late-Hercynian magmatic and metamorphic events. Tectonophysics 182:91–102

Capedri S (1971) Sulle rocce della formazione basica Ivrea–Verbano. 2. Petrografia delle granuliti e rocce derivate nella Val Mastallone (Vercelli) e loro evoluzione petrogenetica. Memorie della Società Geologica Italiana 10:277–312

Cherniak DJ, Watson EB (2000) Pb diffusion in zircon. Chem Geol 172:5–24

Cherniak DJ, Watson EB (2003) Diffusion in Zircon. Rev Mineral Geochem 53:113–143

Corfu F, Hanchar JM, Hoskin PW, Kinny P (2003) Atlas of Zircon Textures. Rev Mineral Geochem 53:469–500

Degeling H, Eggins S, Ellis DJ (2001) Zr budgets for metamorphic reactions, and the formation of zircon from garnet breakdown. Mineral Mag 65:749–758

Diener JF, White RW, Link K, Dreyer TS, Moodley A (2013) Clockwise, low-P metamorphism of the Aus granulite terrain, southern Namibia, during the Mesoproterozoic Namaqua Orogeny. Precambr Res 224:629–652

Ewing RC, Meldrum A, Wang L, Weber WJ, Corrales LR (2003) Radiation Effects in Zircon. Rev Mineral Geochem 53:387–425

Ewing TA, Hermann J, Rubatto D (2013) The robustness of the Zr-in-rutile and Ti-in-zircon thermometers during high-temperature metamorphism (Ivrea-Verbano Zone, northern Italy). Contrib Miner Petrol 165:757–779

Flowers RM, Schmitt AK, Grove M (2010) Decoupling of U–Pb dates from chemical and crystallographic domains in granulite facies zircon. Chem Geol 270:20–30

Fountain DM (1976) The Ivrea–Verbano and Strona–Ceneri zones, northern Italy: a cross-section of the continental crust—new evidence from seismic velocities. Tectonophysics 33:145–165

Fountain DM (1989) Growth and modification of lower continental crust in extended terrains: the role of extension and magmatic underplating. In: Mereu RF, Mueller S, Fountain DM (eds) Properties and processes of earth's lower crust. American Geophysical Union, Washington, DC, pp 287–299

Fraser G, Ellis D, Eggins S (1997) Zirconium abundance in granulite-facies minerals, with implications for zircon geochronology in high-grade rocks. Geology 25:607–610

Geisler T, Pidgeon RT, van Bronswijk W, Kurtz R (2002) Transport of uranium, thorium, and lead in metamict zircon under low-temperature hydrothermal conditions. Chem Geol 191:141–154

Geisler T, Schaltegger U, Tomaschek F (2007) Re-equilibration of zircon in aqueous fluids and melts. Elements 3:43–50

Guillong M, Meier DL, Allan MM, Heinrich CA, Yardley BW (2008) Appendix A6: SILLS: a MatLab-based program for the reduction of Laser Ablation ICP-MS data of homogeneous materials and inclusions. Mineral Assoc Can Short Course 40:328–333

Handy MR (1986) The structure and rheological evolution of the Pogallo Fault Zone, a deep crustal dislocation in the Southern Alps of Northwestern Italy. PhD thesis, University Basel, Switzerland

Handy MR (1987) The structure, age and kinematics of the Pogallo Fault Zone; Southern Alps, northwestern Italy. Eclogae Geol Helv 80:593–632

Handy MR, Franz L, Heller F, Janott B, Zurbriggen R (1999) Multistage accretion and exhumation of the continental crust (Ivrea crustal section, Italy and Switzerland). Tectonics 18:1154–1177

Harley SL, Kelly NM, Möller A (2007) Zircon behaviour and the thermal histories of mountain chains. Elements 3:25–30

Henk A, Franz L, Teufel S, Oncken O (1997) Magmatic underplating, extension, and crustal reequilibration: insights from a cross-section through the Ivrea Zone and Strona-Ceneri Zone, Northern Italy. J Geol 105:367–377

Hermann J, Rubatto D (2003) Relating zircon and monazite domains to garnet growth zones: age and duration of granulite facies metamorphism in the Val Malenco lower crust. J Metamorph Geol 21:833–852

Hofmann AE, Valley JW, Watson EB, Cavosie AJ, Eiler JM (2009) Sub-micron scale distributions of trace elements in zircon. Contrib Miner Petrol 158:317–335

Hoskin PW (2000) Patterns of chaos: fractal statistics and the oscillatory chemistry of zircon. Geochim Cosmochim Acta 64:1905–1923

Hoskin PW, Black LP (2000) Metamorphic zircon formation by solid-state recrystallization of protolith igneous zircon. J Metamorph Geol 18:423–439

Hoskin PW, Schaltegger U (2003) The Composition of Zircon and Igneous and Metamorphic Petrogenesis. Rev Mineral Geochem 53:27–62

Jackson SE, Pearson NJ, Griffin WL, Belousova EA (2004) The application of laser ablation-inductively coupled plasma-mass spectrometry to in situ U–Pb zircon geochronology. Chem Geol 211:47–69

Kelly NM, Harley SL (2005) An integrated microtextural and chemical approach to zircon geochronology: refining the Archaean history of the Napier Complex, east Antarctica. Contrib Miner Petrol 149:57–84

Kelsey DE, Powell R (2011) Progress in linking accessory mineral growth and breakdown to major mineral evolution in metamorphic rocks: a thermodynamic approach in the Na_2O-CaO-K_2O-FeO-MgO-Al_2O_3-SiO_2-H_2O-TiO_2-ZrO_2 system. J Metamorph Geol 29:151–166

Kelsey DE, Clark C, Hand M (2008) Thermobarometric modelling of zircon and monazite growth in melt-bearing systems: examples using model metapelitic and metapsammitic granulites. J Metamorph Geol 26:199–212

Klötzli US, Sinigoi S, Quick JE, Demarchi G, Tassinari CC, Sato K, Günes Z (2014) Duration of igneous activity in the Sesia Magmatic System and implications for high-temperature metamorphism in the Ivrea-Verbano deep crust. Lithos 206–207:19–33

Kohn M, Corrie S, Markley C (2015) The fall and rise of metamorphic zircon. Am Miner 100:897–908

Korhonen FJ, Clark C, Brown M, Bhattacharya S, Taylor R (2013) How long-lived is ultrahigh temperature (UHT) metamorphism? Constraints from zircon and monazite geochronology in the Eastern Ghats orogenic belt, India. Precambr Res 234:322–350

Kunz BE, Johnson TE, White RW, Redler C (2014) Partial melting of metabasic rocks in Val Strona di Omegna, Ivrea Zone, northern Italy. Lithos 190–191:1–12

Kunz BE, Manzotti P, von Niederhäusern B, Engi M, Darling JR, Giuntoli F, Lanari P (2018) Permian high-temperature metamorphism in the Western Alps (NW Italy). Int J Earth Sci 107:203–229

Kusiak MA, Whitehouse MJ, Wilde SA, Nemchin AA, Clark C (2013a) Mobilization of radiogenic Pb in zircon revealed by ion imaging: Implications for early Earth geochronology. Geology 41:291–294

Kusiak MA, Whitehouse MJ, Wilde SA, Dunkley DJ, Menneken M, Nemchin AA, Clark C (2013b) Changes in zircon chemistry during Archean UHT metamorphism in the Napier Complex, Antarctica. Am J Sci 313:933–967

Langone A, José APN, Ji WQ, Zanetti A, Mazzucchelli M, Tiepolo M, Giovanardi T, Bonazzi M (2017) Ductile–brittle deformation effects on crystal-chemistry and U–Pb ages of magmatic and metasomatic zircons from a dyke of the Finero Mafic Complex (Ivrea–Verbano Zone, Italian Alps). Lithos 284:493–511

Luvizotto GL, Zack T (2009) Nb and Zr behavior in rutile during high-grade metamorphism and retrogression: an example from the Ivrea-Verbano Zone. Chem Geol 261:303–317

McDonough WF, Sun SS (1995) The composition of the Earth. Chem Geol 120:223–253

McFarlane CR, Connelly JN, Carlson WD (2005) Intracrystalline redistribution of Pb in zircon during high-temperature contact metamorphism. Chem Geol 217:1–28

McFarlane CR, Connelly JN, Carlson WD (2006) Contrasting response of monazite and zircon to a high-T thermal overprint. Lithos 88:135–149

Mehnert KR (1975) The Ivrea Zone: A model of the deep crust. Neues Jahrbuch Mineralogische Abhandlungen 125:156–199

Mezger K, Krogstad EJ (1997) Interpretation of discordant U–Pb zircon ages: an evaluation. J Metamorph Geol 15:127–140

Möller A, O'Brien PJ, Kennedy A, Kröner A (2003) Linking growth episodes of zircon and metamorphic textures to zircon chemistry: an example from the ultrahigh-temperature granulites of Rogaland (SW Norway). Geological Society, London, 220:65–81 (**Special Publications**)

Monjoie P, Bussy F, Schaltegger U, Mulch A, Lapierre H, Pfeifer H-R (2007) Contrasting magma types and timing of intrusion in the Permian layered mafic complex of Mont Collon (Western Alps, Valais, Switzerland): evidence from U/Pb zircon and $^{40}Ar/^{39}Ar$ amphibole dating. Swiss J Geosci 100:125–135

Mulch A, Cosca M, Handy M (2002a) In-situ UV-laser $^{40}Ar/^{39}Ar$ geochronology of a micaceous mylonite: an example of defect-enhanced argon loss. Contrib Miner Petrol 142:738–752

Mulch A, Rosenau M, Doerr W (2002b) The age and structure of dikes along the tectonic contact of the Ivrea-Verbano and Strona-Ceneri Zones (southern Alps, Northern Italy, Switzerland). Schweiz Mineral Petrogr Mitt 82:55–76

Nasdala L, Wenzel M, Vavra G, Irmer G, Wenzel T, Kober B (2001) Metamictisation of natural zircon: accumulation versus thermal annealing of radioactivity-induced damage. Contrib Miner Petrol 141:125–144

Nasdala L, Lengauer CL, Hanchar JM, Kronz A, Wirth R, Blanc P, Kennedy AK, Seydoux-Guillaume A-M (2002) Annealing radiation damage and the recovery of cathodoluminescence. Chem Geol 191:121–140

Pape J, Mezger K, Robyr M (2016) A systematic evaluation of the Zr-in-rutile thermometer in ultra-high temperature (UHT) rocks. Contrib Miner Petrol 171:44

Paton C, Woodhead JD, Hellstrom JC, Hergt JM, Greig A, Maas R (2010) Improved laser ablation U–Pb zircon geochronology through robust downhole fractionation correction. Geochem Geophys Geosyst 11:Q0AA06

Paton C, Hellstrom J, Paul B, Woodhead J, Hergt J (2011) Iolite: freeware for the visualisation and processing of mass spectrometric data. J Anal At Spectrom 26:2508–2518

Pearce NJ, Perkins WT, Westgate JA, Gorton MP, Jackson SE, Neal CR, Chenery SP (1997) A compilation of new and published major and trace element data for NIST SRM 610 and NIST SRM 612 glass reference materials. Geostand Geoanal Res 21:115–144

Peressini G, Quick JE, Sinigoi S, Hofmann AW, Fanning M (2007) Duration of a large mafic intrusion and heat transfer in the lower crust: a SHRIMP U–Pb Zircon Study in the Ivrea-Verbano Zone (Western Alps, Italy). J Petrol 48:1185–1218

Peterman EM, Reddy SM, Saxey DW, Snoeyenbos DR, Rickard WDA, Fougerouse D, Kylander-Clark ARC (2016) Nanogeochronology of discordant zircon measured by atom probe microscopy of Pb-enriched dislocation loops. Sci Adv 2(9) e1601318

Petrus JA, Kamber BS (2012) VizualAge: a novel approach to laser ablation ICP-MS U–Pb geochronology data reduction. Geostand Geoanal Res 36:247–270

Piazolo S, La Fontaine A, Trimby P, Harley S, Yang L, Armstrong R, Cairney JM (2016) Deformation-induced trace element redistribution in zircon revealed using atom probe tomography. Nat Commun 7:10490

Pidgeon RT (2014) Zircon radiation damage ages. Chem Geol 367:13–22

Quick JE, Sinigoi S, Mayer A (1994) Emplacement dynamics of a large mafic intrusion in the lower crust, Ivrea-Verbano Zone, northern Italy. J Geophys Res: Solid Earth 99:21559–21573

Quick JE, Sinigoi S, Mayer A (1995) Emplacement of mantle peridotite in the lower continental crust, Ivrea-Verbano zone, northwest Italy. Geology 23:739–742

Quick JE, Sinigoi S, Snoke AW, Kalakay TJ, Mayer A, Peressini G (2003) Geologic map of the southern Ivrea-Verbano zone, northwestern Italy. USGS I-2776. U.S. Geological Survey, Reston, VA, pp 1–22. https://pubs.er.usgs.gov/publication/i2776

Reddy SM, Timms NE, Trimby P, Kinny PD, Buchan C, Blake K (2006) Crystal-plastic deformation of zircon: a defect in the assumption of chemical robustness. Geology 34:257–260

Redler C, Johnson TE, White RW, Kunz BE (2012) Phase equilibrium constraints on a deep crustal metamorphic field gradient: metapelitic rocks from the Ivrea Zone (NW Italy). J Metamorph Geol 30:235–254

Redler C, White RW, Johnson TE (2013) Migmatites in the Ivrea Zone (NW Italy): constraints on partial melting and melt loss in metasedimentary rocks from Val Strona di Omegna. Lithos 175:40–53

Regis D, Acosta-Gongora P, Davis WJ, Knox B, Pehrsson SJ, Martel E, Hulbert L (2017) Evidence for Neoarchean Ni-Cu-bearing mafic intrusions along a major lithospheric structure: a case study from the south Rae craton (Canada). Precambr Res 302:312–339

Rivalenti G, Garuti G, Rossi A (1975) The origin of the Ivrea-Verbano basic formation (western Italian Alps); whole rock geochemistry. Bollettino della Societa geologica italiana 94:1149–1186

Rivalenti G, Garuti G, Rossi A, Siena F, Sinigoi S (1981) Existence of different peridotite types and of a layered igneous complex in the Ivrea Zone of the Western Alps. J Petrol 22:127–153

Roberts MP, Finger F (1997) Do U–Pb zircon ages from granulites reflect peak metamorphic conditions? Geology 25:319–322

Rubatto D (2002) Zircon trace element geochemistry: partitioning with garnet and the link between U–Pb ages and metamorphism. Chem Geol 184:123–138

Rubatto D (2017) Zircon: the metamorphic mineral. Rev Mineral Geochem 83:261–295

Rubatto D, Gebauer D (2000) Use of cathodoluminescence for U–Pb zircon dating by ion microprobe: some examples from the Western Alps. In: Pagel M, Barbin V, Blanc P, Ohnenstetter D (eds) Cathodoluminescence in geosciences. Springer, Berlin, Heidelberg, pp 373–400

Rubatto D, Williams IS, Buick IS (2001) Zircon and monazite response to prograde metamorphism in the Reynolds Range, central Australia. Contrib Miner Petrol 140:458–468

Rubatto D, Hermann J, Buick IS (2006) Temperature and bulk composition control on the growth of monazite and zircon during low-pressure anatexis (Mount Stafford, central Australia). J Petrol 47:1973–1996

Rutter E, Brodie K, James T, Burlini L (2007) Large-scale folding in the upper part of the Ivrea-Verbano zone, NW Italy. J Struct Geol 29:1–17

Schaltegger U, Brack P (2007) Crustal-scale magmatic systems during intracontinental strike-slip tectonics: U, Pb and Hf isotopic constraints from Permian magmatic rocks of the Southern Alps. Contrib Miner Petrol 96:1131–1151

Schaltegger U, Fanning CM, Günther D, Maurin JC, Schulmann K, Gebauer D (1999) Growth, annealing and recrystallization of zircon and preservation of monazite in high-grade metamorphism: conventional and isn-situ U–Pb isotope, cathodoluminescence and microchemical evidence. Contrib Miner Petrol 134:186–201

Schaltegger U, Desmurs L, Manatschal G, Müntener O, Meier M, Frank M, Bernoulli D (2002) The transition from rifting to seafloor spreading within a magma-poor rifted margin: field and isotopic constraints. Terra Nova 14:156–162

Schaltegger U, Ulianov A, Müntener O, Ovtcharova M, Peytcheva I, Vonlanthen P, Vennemann T, Antognini M, Girlanda F (2015) Megacrystic zircon with planar fractures in miaskite-type nepheline pegmatites formed at high pressures in the lower crust (Ivrea Zone, southern Alps, Switzerland). Am Miner 100:83–94

Schiøtte L, Compston W, Bridgwater D (1989) Ion probe U-Th-Pb zircon dating of polymetamorphic orthogneisses from northern Labrador, Canada. Can J Earth Sci 26:1533–1556

Schmid SM (1993) Ivrea Zone and Adjacent Southern Alpine Basement. In: von Raumer JF, Neubauer F (eds) Pre-Mesozoic geology in the Alps. Springer, Berlin, pp 567–585

Schmid SM, Zingg A, Handy M (1987) The kinematics of movements along the Insubric Line and the emplacement of the Ivrea Zone. Tectonophysics 135:47–66

Schnetger B (1994) Partial melting during the evolution of the amphibolite- to granulite-facies gneisses of the Ivrea Zone, northern Italy. Chem Geol 113:71–101

Schuster R, Stüwe K (2008) Permian metamorphic event in the Alps. Geology 36:603–606

Seydoux-Guillaume A-M, Bingen B, Paquette J-L, Bosse V (2015) Nanoscale evidence for uranium mobility in zircon and the discordance of U–Pb chronometers. Earth Planet Sci Lett 409:43–48

Sinigoi S, Antonini P, Demarchi G, Longinelli A, Mazzucchelli M, Negrini L, Rivalenti G (1991) Intractions of mantle and crustal magmas in the southern part of the Ivrea Zone (Italy). Contrib Miner Petrol 108:385–395

Sinigoi S, Quick JE, Mayer A, Budahn J (1996) Influence of stretching and density contrasts on the chemical evolution of continental magmas: an example from the Ivrea-Verbano Zone. Contrib Miner Petrol 123:238–250

Sinigoi S, Quick JE, Demarchi G, Klötzli U (2011) The role of crustal fertility in the generation of large silicic magmatic systems triggered by intrusion of mantle magma in the deep crust. Contrib Miner Petrol 162:691–707

Sláma J, Košler J, Condon DJ, Crowley JL, Gerdes A, Hanchar JM, Horstwood MSA, Morris GA, Nasdala L, Norberg N, Schaltegger U, Schoene B, Tubrett MN, Whitehouse MJ (2008) Plešovice zircon—a new natural reference material for U–Pb and Hf isotopic microanalysis. Chem Geol 249:1–35

Taylor RJ, Kirkland CL, Clark C (2016) Accessories after the facts: constraining the timing, duration and conditions of high-temperature metamorphic processes. Lithos 264:239–257

Tichomirowa M, Whitehouse MJ, Nasdala L (2005) Resorption, growth, solid state recrystallisation, and annealing of granulite facies zircon—a case study from the Central Erzgebirge, Bohemian Massif. Lithos 82:25–50

Timms NE, Reddy SM (2009) Response of cathodoluminescence to crystal-plastic deformation in zircon. Chem Geol 261:12–24

Timms NE, Kinny PD, Reddy SM, Evans K, Clark C, Healy D (2011) Relationship among titanium, rare earth elements, U–Pb ages and deformation microstructures in zircon: Implications for Ti-in-zircon thermometry. Chem Geol 280:33–46

Tomaschek F, Kennedy AK, Villa IM, Lagos M, Ballhaus C (2003) Zircons from Syros, Cyclades, Greece—recrystallization and mobilization of zircon during high-pressure metamorphism. J Petrol 44:1977–2002

Valley JW, Cavosie AJ, Ushikubo T, Reinhard DA, Lawrence DF, Larson DJ, Clifton PH, Kelly TF, Wilde SA, Moser DE (2014) Hadean age for a post-magma-ocean zircon confirmed by atom-probe tomography. Nat Geosci 7:219–223

Vavra G, Gebauer D, Schmid R, Compston W (1996) Multiple zircon growth and recrystallization during polyphase Late Carboniferous to Triassic metamorphism in granulites of the Ivrea Zone (Southern Alps): an ion microprobe (SHRIMP) study. Contrib Miner Petrol 122:337–358

Vavra G, Schmid R, Gebauer D (1999) Internal morphology, habit and U-Th-Pb microanalysis of amphibolite-to-granulite facies zircons: geochronology of the Ivrea Zone (Southern Alps). Contrib Miner Petrol 134:380–404

Vonlanthen P, Fitz Gerald JD, Rubatto D, Hermann J (2012) Recrystallization rims in zircon (Valle d'Arbedo, Switzerland): an integrated cathodoluminescence, LA-ICP-MS, SHRIMP, and TEM study. Am Miner 97:369–377

Vorhies SH, Ague JJ, Schmitt AK (2013) Zircon growth and recrystallization during progressive metamorphism, Barrovian zones, Scotland. Am Miner 98:219–230

Voshage H, Hofmann AW, Mazzucchelli M, Rivalenti G, Sinigoi S, Raczek I, Demarchi G (1990) Isotopic evidence from the Ivrea Zone for a hybrid lower crust formed by magmatic underplating. Nature 347:731–736

Watson EB, Harrison TM (1983) Zircon saturation revisited: temperature and composition effects in a variety of crustal magma types. Earth Planet Sci Lett 64:295–304

Watson EB, Wark DA, Thomas JB (2006) Crystallization thermometers for zircon and rutile. Contrib Miner Petrol 151:413–433

Whitehouse MJ, Ravindra Kumar GR, Rimša A (2014) Behaviour of radiogenic Pb in zircon during ultrahigh-temperature metamorphism: an ion imaging and ion tomography case study from the Kerala Khondalite Belt, southern India. Contrib Miner Petrol 168:1–18

Williams IS (1992) Some observations on the use of zircon U–Pb geochronology in the study of granitic rocks. Transac R Soc Edinburgh: Earth Sci 83:447–458

Williams IS (2001) Response of detrital zircon and monazite, and their U–Pb isotopic systems, to regional metamorphism and host-rock partial melting, Cooma Complex, southeastern Australia. Aust J Earth Sci 48:557–580

Yakymchuk C, Brown M (2014) Behaviour of zircon and monazite during crustal melting. J Geol Soci Lond 171:465–479

Zanetti A, Mazzucchelli M, Sinigoi S, Giovanardi T, Peressini G, Fanning M (2013) SHRIMP U–Pb zircon Triassic intrusion age of the Finero Mafic Complex (Ivrea-Verbano Zone, Western Alps) and its geodynamic implications. J Petrol 54:2235–2265

Zingg A (1978) Regionale Metamorphose in der Ivrea Zone (Nord-Italien). PhD thesis, ETH Zürich, Switzerland

Zingg A (1980) Regional metamorphism in the Ivrea Zone (Southern Alps, N-Italy): field and microscopic Investigations. Schweiz Mineral Petrogr Mitt 60:153–179

Zingg A, Handy MR, Hunziker JC, Schmid SM (1990) Tectonometamorphic history of the Ivrea Zone and its relationship to the crustal evolution of the Southern Alps. Tectonophysics 182:169–192